Chapter 3

Theory of Extracellular Electrical Stimulation

In Chapter 2, a functional description of the retinal implant was given. Central to the implant's function is the task of creating action potentials in ganglion cell bodies where the retinal circuitry has failed to do so. The purpose of this chapter is to investigate a general theory of how such a task is accomplished.

Definition of terms

When an action potential is created in a nerve cell, the cell is said to be *stimulated*. Nerve cells in living organisms may be stimulated by electrical, mechanical, or chemical means, depending on the particular cell type. *Electrical stimulation* of many types of cells may be performed by applying an electrical current inside or near the cells. If current is applied directly to the inside of a cell and an action potential is generated as a result, the cell is stimulated *intracellularly* (see Figure 3-1a). If the stimulating current is applied outside of a cell, as in Figure 3-1b, the cell is stimulated *extracellularly*.

The retinal implant will use electrical current to stimulate ganglion cells in the retina. For a variety of reasons, the implant electrodes will not penetrate the retinal cells. Therefore, the retinal implant's mode of operation is *extracellular electrical stimulation*.

Previous work

A number of papers have been written on extracellular electrical stimulation. Broadly speaking, research in the field has been either experimentally or analytically motivated. Research of the first type has generally involved experiments performed on real nerve cells to test or formulate qualitative theories which describe how the cells were stimulated. A useful summary of the data and theories emanating from such research is given by Ranck[46]. Research of the second type is more mathematical and abstract. Models of nerve cells have been constructed based on some particular set of assumptions about cell shape, membrane structure, and environment. Due to the many assumptions that must be made to simplify analysis, few attempts have been made at finding quantitative correspondences between theory and experiment[48, 51, 53]. For the most part, analyses have been matched qualitatively to familiar trends in extracellular electrical stimulation experiments, or have predicted phenomena which remain untested[8, 33, 41, 52, 47, 61].

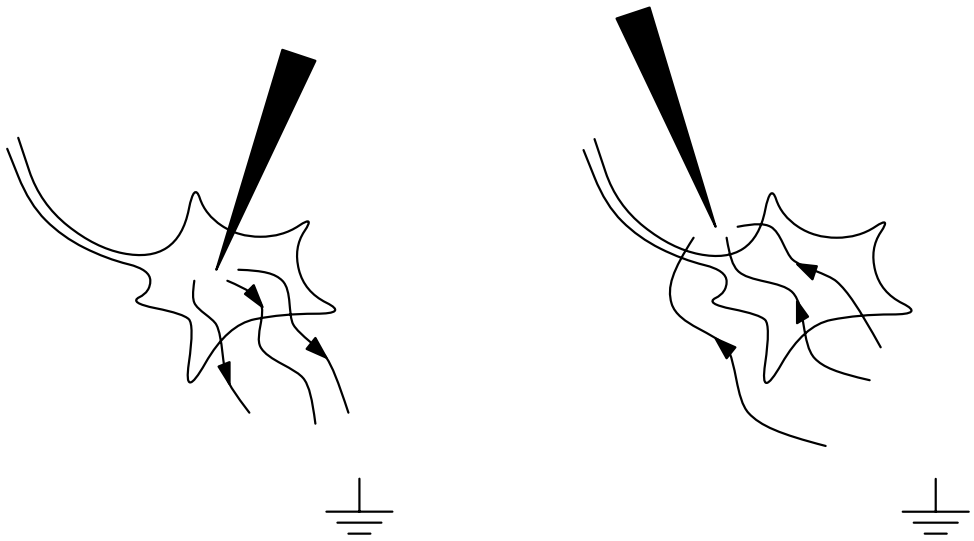

Figure 3-1: (a) Schematic of intracellular stimulation of a cell; (b) Schematic of extracellular stimulation of a cell.

The work of the analytical literature is divided into two parts based on morphological considerations. While the typically bulbous cell body of a nerve cell has been modeled as a perfect sphere, the shaft-like axon has been modeled as a right circular cylinder. To my knowledge, dendrites have not been modeled for extracellular electrical stimulation problems. Spherical cell body models and cylindrical axon models have been analyzed in isolation in order to simplify the math. That is, axon models have been analyzed in the absence of a cell body, and cell body models have been analyzed in the absence of an axon. For reasons that will become clear later in the chapter, analyses of axon models have concentrated on the effects of longitudinal variations in electric potential and largely ignored transverse effects. The analytical methods which have been used to study longitudinal effects in axons and to study cell bodies are now briefly considered.

A general method for analyzing the effects of variations in electric potential along an axon's length is the procedure used by McNeal[33]. The first step of McNeal's method is to calculate the potentials created in the extracellular space by a specified electrode configuration. A familiar configuration is the monopolar spherical geometry. The extracellular medium is commonly assumed to be a uniform, linear, and isotropic conductor of infinite extent. Due to its relatively small size, the axon model is assumed to have negligible effect on the electrode-induced potentials, and is usually ignored during this step. For relatively simple models based on the assumptions described above, closed-form solutions for the extracellular potentials have been found. For more complex models, numerical simulations could be employed to find the extracellular potentials.

Once the electrode-induced potentials are known, an axon model must be chosen. All such models rely on the basic set of assumptions listed in Table 3.1. Implicit in assumptions 2 and 5 is the notion that the electric field creates a radially symmetric equipotential region outside of the axon model at a given position along its length. For most electrode configurations, this will not be strictly true. However, it has been demonstrated by McNeal

1. The cell membrane is a cylindrical boundary that surrounds a conductor of electrical current, the intracellular solution, which is assumed to be homogeneous, isotropic, and obey Ohm's law.
2. All the electric variables have cylindrical symmetry.
3. A circuit theory description of currents and voltages is adequate. That is, the quasi-static terms of Maxwell's equations are sufficient, and electromagnetic radiation effects are negligible.
4. Current flows through the inner conductor in the longitudinal direction only. Current flows through the membrane in the radial direction only.
5. At a given longitudinal position along the axon, the inner conductor and external surface of the axonal membrane are equipotentials, so that the only variation in potential occurs in the radial direction, across the membrane.

Table 3.1: Basic assumptions for analyzing longitudinal effects in axons; adapted from [63].

that the effects of transverse variations in extracellular potential were vastly smaller to those of variations in potential along the axon's length[33]. This fact will also be demonstrated later in the chapter.

In addition to the general assumptions listed in Table 3.1, several specific attributes must be added to the axon model before the second step of McNeal's method can be carried out. For instance, one must decide if the model is to represent a myelinated or an unmyelinated axon. In addition, an axonal length - be it finite or infinite - must be specified. Furthermore, membrane properties such linearity and passivity, as exhibited by the cable model, or nonlinearity, as seen in the Hodgkin/Huxley model of the squid axon[21] must be decided. Finally, the time-dependent behavior of the model must be considered. Will we analyze a steady-state response of a model, a transient effect, or a frequency response? McNeal studied the transient response of two different models of finite-length, myelinated axons to a step of extrinsic current; one model was passive and linear, and the other was the nonlinear Frankenhauser-Huxley model of frog nerve[33].

The second step of McNeal's method is to calculate the transmembrane potentials induced in the axon model by the extracellular potentials determined in the first step. Note from assumption 3 of Table 3.1 that the model generated by each choice of axon model properties will have a circuit theory representation. Once the details of the axon model have been decided, the corresponding circuit is "placed" somewhere in the extracellular medium. The axon model circuit is then solved (either analytically or numerically, depending on the complexity of the circuit) for the case where it is driven by a series of voltage sources connected to the nodes representing the extracellular space along the axon model's length. The voltages at these extracellular nodes are assigned so as to match the voltage profile seen by the axon when placed in the chosen position and orientation relative to the stimulating electrode. The transmembrane potentials can then be easily deduced from the circuit solution.

I have only seen two papers which present models of the cell body for extracellular electrical stimulation problems. In both papers, the cell body is modeled as a perfect sphere with a membrane of zero thickness. Plonsey and Altman attribute a distributed specific resistance (SI units are ohm$\cdot$m^2) to the membrane and use their model to analyze the effects of steady-state electric fields[41], while Cartee and Plonsey attribute both a specific resistance and a capacitance per unit area to the membrane in order to analyze the transient effects of a step in applied electric field[8]. The analyses in the two papers are similar in most other respects. The intracellular and extracellular fluids are modeled as linear, isotropic, and homogeneous conductors. The applied electric field is uniform far away from the cell body model, corresponding to the parallel plate electrode configuration. The electric potential inside of and outside of the cell body model are found by solving Laplace's equation using standard techniques. The uniformity of the field far from the cell body model and the electrical characteristics of the membrane provide the necessary boundary conditions. The transmembrane potential can be calculated from the resulting solution in a straightforward manner. As in the case of the simpler axon models discussed above, useful analytical results can be found in closed form. Unlike the axon models for longitudinal effects, the cell body model plays a role in determining the extracellular potentials created by the extracellular electrode near the cell.

Chapter overview

The simplest of the models described above, incorporating idealized electric fields and cell shapes, uniformly linear membranes, and steady-state conditions will be analyzed in this chapter. Three representative scenarios, illustrated schematically in Figure 3-2, will be examined. In all cases, two large, perfectly conducting parallel plates are connected to a current source which has been on for a long time relative to any time constants of interest. Neglecting fringing, the electric field in the absence of the cell models will be uniform and horizontally directed between the plates, and zero everywhere else. In section 3.2, the transmembrane potentials induced in the spherical cell body model (Figure 3-2a) will be found from Laplacian solutions for the electric potential. In section 3.3, the transmembrane potentials induced in the infinitely long axon by a longitudinal field (Figure 3-2b) will be calculated using McNeal's method in conjunction with the cable model for unmyelinated axons. The mathematical formula for the transmembrane potentials induced in the cell body model will be related to the general principles described by Ranck[46]. Results from the longitudinal axon model will be related to theoretical work presented by various authors. The analyses of these first two stimulus paradigms will be our our primary means of understanding how nerve cells are stimulated extracellularly. The transmembrane potentials induced in the infinitely long axon by a transverse electric field (Figure 3-2c) can be found from Laplacian solutions for the electric potential, as in the case of the spherical cell body model. While this formulation has not yet been seen in the literature, the derivations bear a strong resemblance to those for the spherical cell (see appendix A.2), and consequently yield little additional insight. The solution for this model is given in section 3.4, where analytical results are used to predict how the minimum-amplitude or *threshold* fields required to generate action potentials using the three stimulus paradigms compare with one another.

The goal of the analyses that follow is to predict as many general phenomena of extracellular electrical stimulation of nerve cells as possible with relatively simple models. This, of course, involves tradeoffs. Due to the large number of assumptions that will be made in modeling cell bodies and axons, the analyses that follow will fail to predict significant aspects of nerve cell behavior. Section 3.1 provides a formal statement of the assumptions made in this chapter. A discussion of the more dramatic consequences of certain assumptions is included in that section. The topic is then reconsidered more thoroughly at the end of the chapter, in section 3.5.

It should also be noted that the models we are proposing may apply to more general situations than those that will be analyzed in this thesis. For example, induced transmembrane potentials in all models may be found for *arbitrary* electrode configurations if numerical simulations are employed. Furthermore, all models take the cell membrane capacitance into account, so that equations derived from the models can be used to evaluate the effects of low frequency time varying fields[1].

3.1 Statement of Assumptions

In addition to the assumptions listed in Table 3.1 for modeling longitudinal effects in axons, the following will be assumed:

[1]Of course, if the time variation of the electric field is rapid enough to produce electromagnetic radiation effects, the models presented in this chapter will be inadequate.

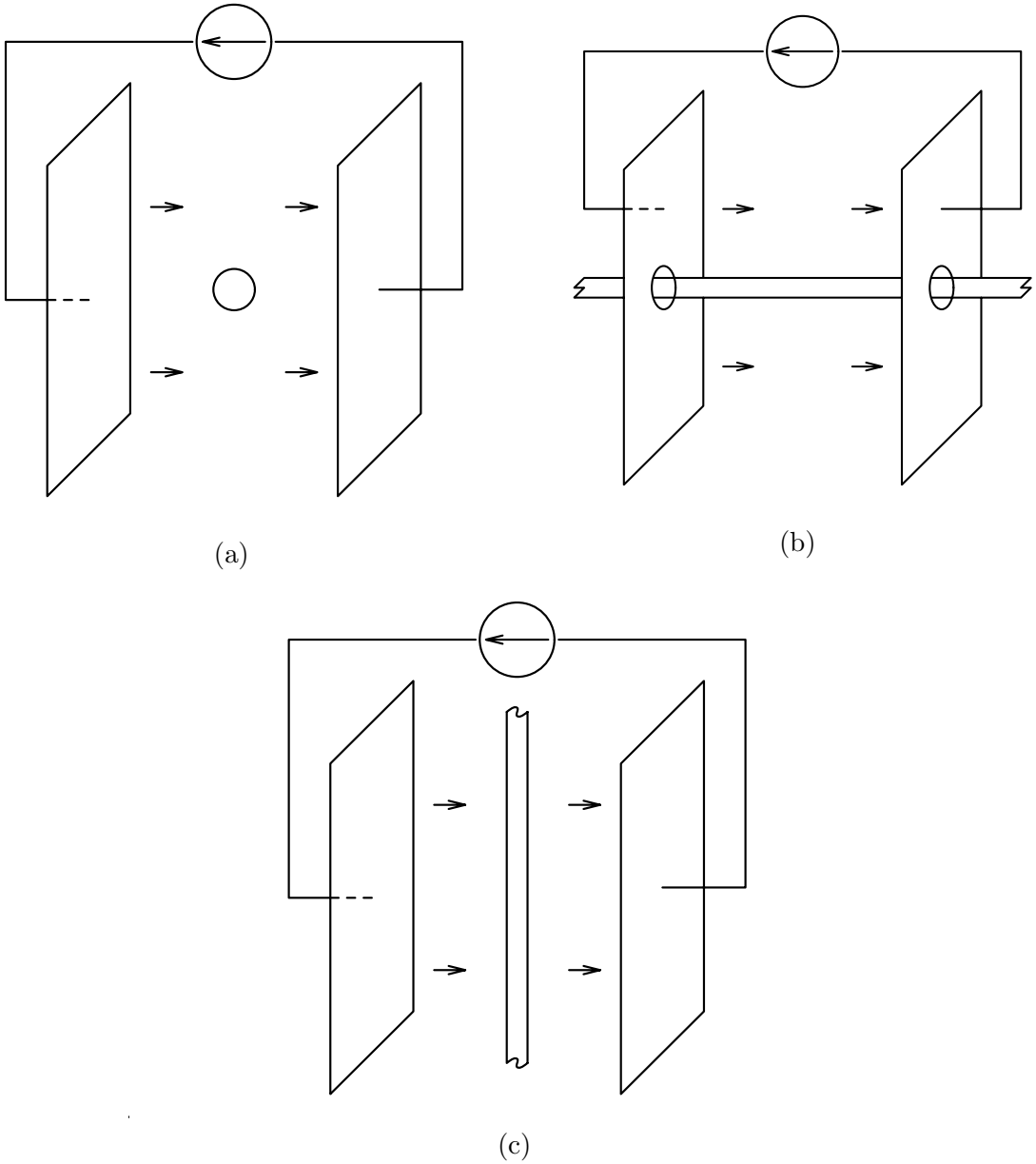

Figure 3-2: Stimulus paradigms. (a) Cell body in a uniform field; (b) Axon in a longitudinal field; (c) Axon in a uniform, transverse field.

1. Extracellular electric fields near a cell body are not affected by the cell's axon, by the cell's dendrites, or by other cells in the vicinity; extracellular fields near an axon are not affected by the cell body, by the cell's dendrites, or by other cells. In other words, cell body and axon models will be analyzed in isolation.

2. Cell bodies are perfect spheres. Axons are right circular cylinders of (doubly) infinite length.

3. Intracellular and extracellular fluids have linear, isotropic, and homogeneous electrical properties.

4. Below a fixed threshold depolarization, cell membranes have passive, linear, and time-invariant electrical properties which are uniform over their entire surface area.

5. There are no fixed charges in the material, so that the electric potential has Laplacian solutions.

6. When electroquasistatic models are used, the applied electric field is uniform far from the cell body and axon models.

7. When circuit models are used, extracellular electrodes are represented with perfect voltage sources whose values are determined by the potentials induced by the electrode in a homogeneous extracellular medium.

Some of the assumptions are stronger than others, and all will have an effect on the validity of the derived results. Probably the strongest of the assumptions is that cell membranes are passive and linear. This assumption has two important consequences. First, nerve cell membranes have active components such as the sodium-potassium pump, which helps maintain a *rest* potential across the membrane. The inside of a resting cell is generally at a lower potential than the outside of the cell, and the membrane is said to be *polarized*. Since the models which will be used here have no active components, they will not predict this polarization. Second, nerve cells can produce highly nonlinear *action potentials*. Since the models which used here are linear, they will not reproduce action potentials or any other properties of excitation.

All is not lost, however. For small enough perturbations of transmembrane potential about its rest value, cell membranes are *incrementally* linear [63]. Through their extensive theoretical and experimental work on crustacean axons, for example, Hodgkin and Rushton demonstrated that the cell membrane will behave linearly for stimulating currents up to half of the threshold for excitation[22]. On the other hand, McNeal's numerical simulations of the Frankenhauser-Huxley equations for myelinated frog nerve show that linear behavior persists up to 80% of the excitation threshold[33].

Our models represent a linearization of the membrane's nonlinear electrical properties about the rest potential. Presumably, the linear approximation will be a very good one well below the excitation threshold, and will become progressively worse as the threshold is approached.

The rest potential itself is not accounted for in our models. Derived transmembrane potentials therefore represent incremental deviations about this value. We will speak of *induced* transmembrane potentials when discussing the incremental effect of the applied field. The sign of the induced transmembrane potential will reveal the effective electrophysiological state of the cell model's membrane. In areas where the induced transmembrane

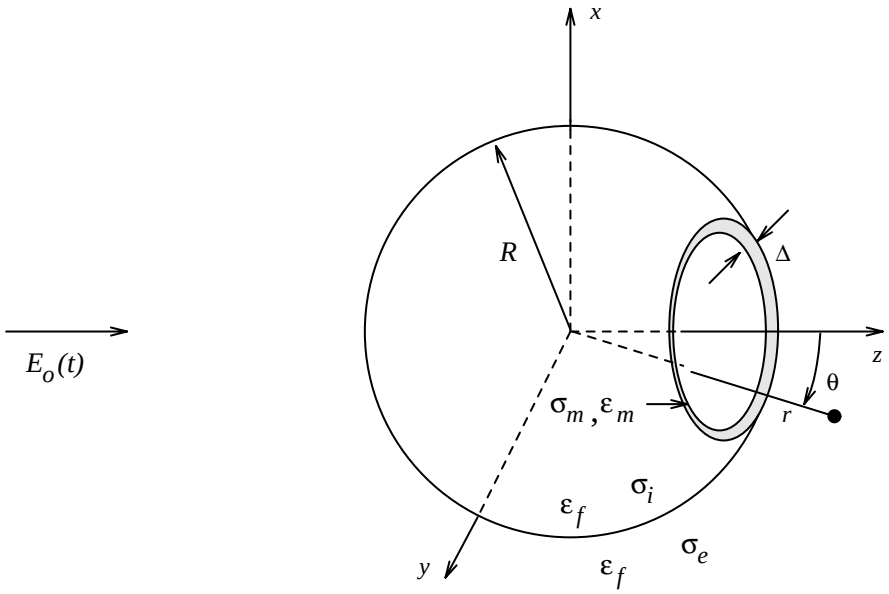

Figure 3-3: Cell body model.

potential is positive, the inside of the cell model is incrementally positive with respect to the outside. Such areas are said to be *depolarized*. In areas where the induced transmembrane potential is negative, the inside of the cell model is incrementally negative with respect to the outside. These areas are said to be *hyperpolarized*.

Excitable cells will produce action potentials if their membranes are sufficiently depolarized. Under assumption 4, linear models may be used to predict excitation thresholds explicitly. It is sufficient to calculate the electric field strength required to induce the threshold depolarization in the models. When the threshold is reached, action potentials are produced and the linear models are no longer valid. For the purposes of this thesis, we are not interested in the properties of the action potentials themselves. Therefore, nonlinear models will not be examined. Furthermore, we are less interested in the exact values of the thresholds for the three stimulus paradigms than in how these thresholds compare with one another. Such relationships will be explored in section 3.4.

3.2 Cell Body in a Uniform Electric Field

A model for the cell body is illustrated in Figure 3-3. The model is a perfect sphere of radius R centered on a coordinate axis with the Cartesian coordinates x, y and z and the spherical coordinates r and θ drawn in for reference. The intracellular and extracellular fluids have uniform permittivity ϵ_f. The intracellular fluid has uniform conductivity σ_i, and the extracellular fluid has uniform conductivity σ_e. The cell membrane is modeled as a linear, isotropic, and homogeneous spherical shell of thickness Δ, permittivity ϵ_m, and conductivity σ_m. The model is similar to that analyzed by Cartee and Plonsey[8], but differs in two respects. First, the membrane thickness Δ is assumed to be zero in their model. In the place of permittivity and conductivity, the zero thickness membrane is described by two distributed circuit parameters, a specific resistance and a capacitance per

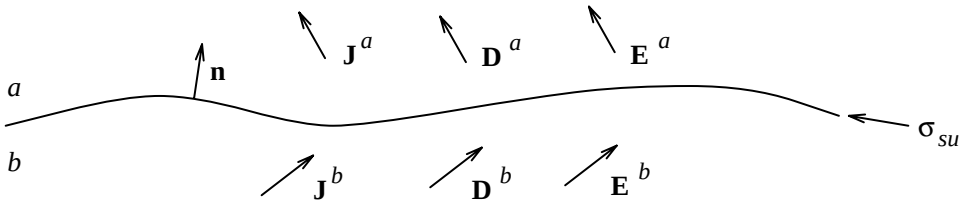

Figure 3-4: Illustration of vectors used for boundary conditions.

unit area. Second, the fluid permittivity ϵ_f is neglected in their model. Laplacian solutions for potentials in and around the model used by Cartee and Plonsey may be found fairly easily using a hybridization of circuit theory and classical electric field theory laws. While requiring slightly more algebra, the model of Figure 3-3 entails fewer assumptions about cell structure and provides a consistent electric field theory representation of the cell body.

3.2.1 Solution form and boundary conditions

The solution for the electric potential is of the form

$$\Phi = \begin{cases} a(t) r \cos\theta & \text{for } r < R, \\ b(t) r \cos\theta + \frac{c(t)}{r^2} \cos\theta & \text{for } R < r < R + \Delta, \\ -E_o(t) r \cos\theta + \frac{d(t)}{r^2} \cos\theta & \text{for } r > R + \Delta. \end{cases} \tag{3.1}$$

Before we determine the boundary conditions that apply to this solution, a few comments are in order. First, notice that for large r, the potential is approximately $-E_o(t) r \cos\theta$ or simply $-E_o(t) z$. This agrees with the previously established condition that the electric field is uniform and horizontally directed far from the cell body model. Second, note that there is no ϕ-variation in the potential. This is due to the uniformity of the applied field and spherical symmetry of the cell body model. More importantly, it points to the relative simplicity of solution (3.1), which for other applied fields and cell body geometries would likely involve a modal expansion in spherical harmonics. Now we will establish the boundary conditions which apply to the solution given above.

The functions $a(t), b(t), c(t)$ and $d(t)$ can be related to one another and to the surface charge densities on the membrane:solution boundaries using three continuity conditions. The conditions follow from, respectively, Faraday's Law, Gauss' Law, and charge conservation:

$$\begin{aligned} \mathbf{n} \times (\mathbf{E}^a - \mathbf{E}^b) &= 0, \\ \mathbf{n} \cdot (\mathbf{D}^a - \mathbf{D}^b) &= \sigma_{su}, \\ \mathbf{n} \cdot (\mathbf{J}_u^a - \mathbf{J}_u^b) &= -\dot{\sigma}_{su} \, . \end{aligned}$$

In above equations, $\mathbf{E}$ is the electric field, $\mathbf{D}$ is the electric flux density, $\mathbf{J}_u$ is the unpaired current density, σ_{su} represents surface charge density, and $\dot{\sigma}_{su}$ is the time derivative of σ_{su}. The vector $\mathbf{n}$ is the unit normal to the boundary. The superscripts ^{a} and ^{b} indicate position with reference to the boundary at which the continuity condition is applied, as shown in Figure 3-4. The cell membrane, intracellular fluid, and extracellular fluid are

all assumed to be linear, isotropic, and homogeneous materials. Thus, the constitutive laws for unpaired current density and displacement flux density may be used on the latter two continuity conditions, yielding

$$\begin{aligned} \mathbf{n} \cdot (\epsilon_a \mathbf{E}^a - \epsilon_b \mathbf{E}^b) &= \sigma_{su}, \\ \mathbf{n} \cdot (\sigma_a \mathbf{E}^a - \sigma_b \mathbf{E}^b) &= -\dot{\sigma_{su}} . \end{aligned}$$

Since the cell body is a perfect sphere centered on the origin, the normal vector to the membrane is $\mathbf{n} = \hat{\imath}_r$. Using this fact and the definition of potential,

$$\mathbf{E} = -\nabla \Phi, \tag{3.2}$$

the continuity conditions take the following form:

$$\frac{\partial \Phi^a}{\partial \theta} = \frac{\partial \Phi^b}{\partial \theta},$$

$$-\epsilon_a \frac{\partial \Phi^a}{\partial r} + \epsilon_b \frac{\partial \Phi^b}{\partial r} = \sigma_{su},$$

$$-\sigma_a \frac{\partial \Phi^a}{\partial r} + \sigma_b \frac{\partial \Phi^b}{\partial r} = -\dot{\sigma_{su}} .$$

Application of the continuity conditions at $r = R$ and $r = R + \Delta$ yield the following equations.

$$bR + \frac{c}{R^2} = aR, \tag{3.3}$$

$$-E_o(t)(R+\Delta) + \frac{d}{(R+\Delta)^2} = b(R+\Delta) + \frac{c}{(R+\Delta)^2}, \tag{3.4}$$

$$-\epsilon_m \left(b - \frac{2c}{R^3} \right) \cos\theta + \epsilon_f a \cos\theta = \sigma^i_{su}, \tag{3.5}$$

$$-\epsilon_f \left[-E_o(t) - \frac{2d}{(R+\Delta)^3} \right] \cos\theta + \epsilon_m \left[b - \frac{2c}{(R+\Delta)^3} \right] \cos\theta = \sigma^e_{su}, \tag{3.6}$$

$$-\sigma_m \left(b - \frac{2c}{R^3} \right) \cos\theta + \sigma_i a \cos\theta = -\dot{\sigma}^i_{su}, \tag{3.7}$$

$$-\sigma_e \left[-E_o(t) - \frac{2d}{(R+\Delta)^3} \right] \cos\theta + \sigma_m \left[b - \frac{2c}{(R+\Delta)^3} \right] \cos\theta = -\dot{\sigma}^e_{su} . \tag{3.8}$$

In the above equations, $a = a(t)$, $b = b(t)$, $c = c(t)$, $d = d(t)$, and σ^i_{su} and σ^e_{su} are the surface charge densities on the intracellular and extracellular membrane:solution boundaries, respectively. These equations completely describe a linear time-invariant system in six variables (a, b, c, d, σ^i_{su}, and σ^e_{su}) which may be solved completely for a given $E_o(t)$.

3.2.2 Time-independent solution

If the applied field is held constant at E_o, and the system described above is in steady state, the time derivatives in equations (3.7) and (3.8) will be zero. In such a case, equa-

tions (3.3),(3.4), (3.7), and (3.8) can be solved for a, b, c, and d.

From equations (3.3) and (3.4), it can be shown that

$$b = a - \frac{(R+\Delta)^3}{(R+\Delta)^3 - R^3}\left[a - \frac{d}{(R+\Delta)^3} + E_o\right], \tag{3.9}$$

$$c = \frac{R^3(R+\Delta)^3}{(R+\Delta)^3 - R^3}\left[a - \frac{d}{(R+\Delta)^3} + E_o\right]. \tag{3.10}$$

Substituting into equations (3.7) and (3.8), noting that the time derivatives are zero, and collecting terms yields

$$a\left[\sigma_i+\sigma_m\frac{2(R+\Delta)^3+R^3}{(R+\Delta)^3-R^3}\right]+\frac{d}{(R+\Delta)^3}\left[-\sigma_m\frac{3(R+\Delta)^3}{(R+\Delta)^3-R^3}\right]=E_o\left[-\sigma_m\frac{3(R+\Delta)^3}{(R+\Delta)^3-R^3}\right],$$

$$a\left[-\sigma_m\frac{3R^3}{(R+\Delta)^3-R^3}\right]+\frac{d}{(R+\Delta)^3}\left[2\sigma_e+\sigma_m\frac{(R+\Delta)^3+2R^3}{(R+\Delta)^3-R^3}\right]=E_o\left[-\sigma_e+\sigma_m\frac{(R+\Delta)^3+2R^3}{(R+\Delta)^3-R^3}\right].$$

Several of the expressions in the two preceding equations can be written in terms of the membrane conductance per unit area,

$$G_m = \sigma_m/\Delta, \tag{3.11}$$

by noting that

$$\frac{\sigma_m}{(R+\Delta)^3 - R^3} = \frac{G_m}{3R^2 + 3R\Delta + \Delta^2}.$$

After making this substitution, we have

$$a\left[\sigma_i+G_m\frac{2(R+\Delta)^3+R^3}{3R^2+3R\Delta+\Delta^2}\right]+\frac{d}{(R+\Delta)^3}\left[-G_m\frac{3(R+\Delta)^3}{3R^2+3R\Delta+\Delta^2}\right]=E_o\left[-G_m\frac{3(R+\Delta)^3}{3R^2+3R\Delta+\Delta^2}\right],$$

$$a\left[-G_m\frac{3R^3}{3R^2+3R\Delta+\Delta^2}\right]+\frac{d}{(R+\Delta)^3}\left[2\sigma_e+G_m\frac{(R+\Delta)^3+2R^3}{3R^2+3R\Delta+\Delta^2}\right]=E_o\left[-\sigma_e+G_m\frac{(R+\Delta)^3+2R^3}{3R^2+3R\Delta+\Delta^2}\right].$$

The equations we have derived thus far can now be greatly simplified by recognizing that membrane thickness Δ is much less than the cell body radius R. Specifically, cell membranes are known to be on the order of 75Å thick[63], whereas the radii of ganglion cell bodies[2] in rabbit retina[3] have been measured at roughly 10μm[1, 26]. Thus the cell body radius is over a factor of 1000 greater than cell membrane thickness. Based on this comparison, we make the approximation $R + \Delta \approx R$ to obtain

$$a(\sigma_i + G_m R) + d\left(-\frac{G_m}{R^2}\right) = E_o(-G_m R),$$

$$a(-G_m R) + d\left(\frac{2\sigma_e}{R^3} + \frac{G_m}{R^2}\right) = E_o(-\sigma_e + G_m R).$$

[2]Of course, retinal ganglion cell bodies are not perfect spheres. Therefore, to speak of cell body "radius" is somewhat misleading. The numbers used here are calculated from measurements of cell body area when viewed under a light microscope, and are used only to demonstrate that cell body size is generally much larger than cell membrane thickness.

[3] At the time this chapter was written, rabbits were the primary animal used for experimental research in the retinal implant group.

Now we can solve for a and d fairly easily, and we find that

$$a = -\frac{3\sigma_e G_m R}{\sigma_i G_m R + 2\sigma_e G_m R + 2\sigma_i \sigma_e} E_o, \tag{3.12}$$

$$d = \frac{\sigma_i G_m R^4 - \sigma_e G_m R^4 - \sigma_i \sigma_e R^3}{\sigma_i G_m R + 2\sigma_e G_m R + 2\sigma_i \sigma_e} E_o. \tag{3.13}$$

Equations (3.1), (3.12) and (3.13) provide a complete solution for the electric potential inside and outside of the cell body model. To determine the potential inside of the cell membrane, it would be necessary to find b and c. This could be done by substituting the solutions for a and d back into equations (3.9) and (3.10). However, the potential inside of the membrane is not of critical importance to this analysis, so we will neglect b and c altogether.

3.2.3 Interpretation of the time-independent solution

For purposes of nerve cell stimulation, the critical effect of an applied field is that it changes the electric potential difference between the inside and the outside of the cell. This effect will be called the *induced transmembrane potential*, and will be defined by

$$V_m = \Phi|_{r=R} - \Phi|_{r=R+\Delta}. \tag{3.14}$$

The potential Φ at a point in space is determined by equations (3.1), (3.12), and (3.13). The particular value V_m takes on depends on where along the cell membrane it is calculated. Due to the symmetry of the cell body model, this position may be described by the angle θ only (see Figure 3-3). As discussed in section 3.1, positive values of V_m will indicate areas of cell membrane which are depolarized, and negative values of V_m will indicate hyperpolarized areas.

Applying the definition of transmembrane potential given by equation (3.14) to the solution found in section 3.2.2 gives

$$\boxed{V_m = \frac{3\sigma_i \sigma_e R}{\sigma_i G_m R + 2\sigma_e G_m R + 2\sigma_i \sigma_e} E_o \cos\theta.} \tag{3.15}$$

This solution agrees with the results of Cartee and Plonsey, who derived the step-response of V_m for a spherical cell body in a uniform field using a similar model[8].

Features of the induced transmembrane potential

While based on highly simplified models, the induced transmembrane potential given by equation (3.15) predicts many of the phenomena described by Ranck for extracellular electrical stimulation of real nerve cells[46]. Mathematical features of the induced transmembrane potential are listed below and accompanied by the related phenomenon reported by Ranck.

- $V_m \propto \cos\theta$

  Regions at the right side of the cell (θ is near zero) are depolarized whereas regions at the left side of the cell (θ is near π) are hyperpolarized. Since the applied electric field points from the left to right, hyperpolarized regions occur where the extracellular potential is relatively high and depolarized regions occur where the extracellular potential is relatively low.

$G_m = 0.001$ S/cm^2
$\sigma_i = 0.005$ S/cm
$\sigma_e = 0.02$ S/cm

Table 3.2: Electrical parameters for a typical cell. From [8].

- $V_m \propto R$ for sufficiently low $G_m R$

  Small cells will suffer smaller induced transmembrane potentials than large cells in the same applied electric field. $G_m R$ will be "sufficiently low" if it is much less than σ_i and σ_e. Using a radius of $R = 10\mu$m and the electrical parameters of a typical cell[8] listed in Table 3.2, we see that $G_m R = 1 \times 10^{-6}$ S/cm. This is at least a factor of 1000 smaller than σ_i or σ_e.

- $V_m \downarrow 0$ as $G_m \uparrow \infty$

  The induced transmembrane potential is greatest for a perfectly insulating ($G_m = 0$) membrane, and decreases as the membrane conductance increases.

- $V_m \propto E_o$

  Larger applied electric fields induce larger transmembrane potential changes. The electric field is defined as the gradient of the electric potential. Therefore, the steeper the extracellular voltage gradient, the greater the induced transmembrane potential.

Potential averaging property

Using the parameters in Table 3.2, a radius of $R = 10\mu$m and an applied electric field $E_o = 1$ V/cm, the plot of Figure 3-5 was produced to illustrate how transmembrane potentials are induced in the cell body model. Potentials in the intracellular and extracellular space are plotted along the z-axis as defined in Figure 3-3. Outside of the cell, $|z| > R$, the potential profiles are approximately straight lines of negative slope, corresponding to the constant electric field that would be established in the absence of the cell body model. Inside the cell, $|z| < R$, the potential is constant and has assumed the average value of the potentials in the neighboring extracellular space. The discontinuities in potential across the dotted lines in Figure 3-5 represent induced transmembrane potentials. At $z = -R$ the interior of the cell model is at a lower potential than the exterior, representing a membrane hyperpolarization. At $z = R$, the interior of the cell model is at a higher potential than the exterior, representing a membrane depolarization.

The potential averaging that takes place inside the cell has a simple circuit theory analogy. A one-dimensional circuit model of the cell body is illustrated in Figure 3-6. Circuit nodes are labeled with circled integers for reference. R_l and R_r represent lumped cell membrane resistances of the left and right halves of the cell body. Voltage drops across these membrane resistances are analogous to induced transmembrane potentials. R_i represents the intracellular resistance. Note that the membrane capacitance has been left out of this model. In steady-state, the capacitances connected in parallel with resistors will

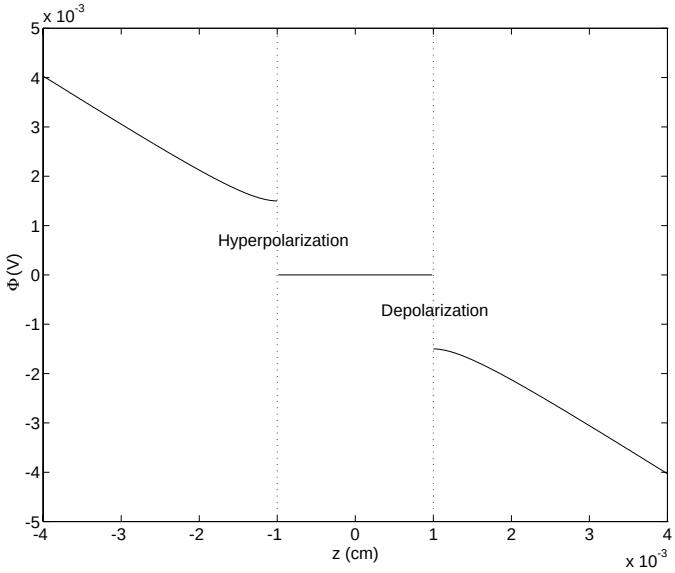

Figure 3-5: Extracellular and intracellular voltages along the z-axis. Dotted lines indicate boundary between the inside and the outside of the cell body model, i.e. the cell membrane.

resemble open circuits, and will therefore not affect the final distribution of voltages in the circuit.

The sources v_l and v_r represent extracellularly applied voltages on the left and right sides of the cell body, respectively. Strictly speaking, extracellular electrodes such as those depicted in Figure 3-2a *will not* behave like perfect voltage sources in the immediate vicinity of a cell, since the cell will play a role in determining the extracellular potentials nearby. To see this relation, recall that the coefficient d in equation (3.1) for the electric potential outside of the cell is shown in equation (3.13) to depend on the cell radius R, the intracellular conductivity σ_i, the extracellular conductivity σ_e, and the membrane conductance per unit area G_m. Assuming the extracellular voltages are known, however, perfect sources may be substituted at the appropriate nodes of the circuit to model the effect of extracellular electrodes.

The intracellular voltages at nodes ② and ③ may be found by solving the circuit equations. These voltages are given by

$$v_2 = v_r + \frac{R_i + R_r}{R_l + R_i + R_r}(v_l - v_r),$$

$$v_3 = v_r + \frac{R_r}{R_l + R_i + R_r}(v_l - v_r).$$

If the intracellular resistance is small and the membrane resistances are equal,

$$v_2 \approx v_3 \approx \frac{v_r + v_l}{2}.$$

Thus, the potentials at the intracellular nodes ② and ③ are the average value of the potentials at the extracellular nodes ① and ④.

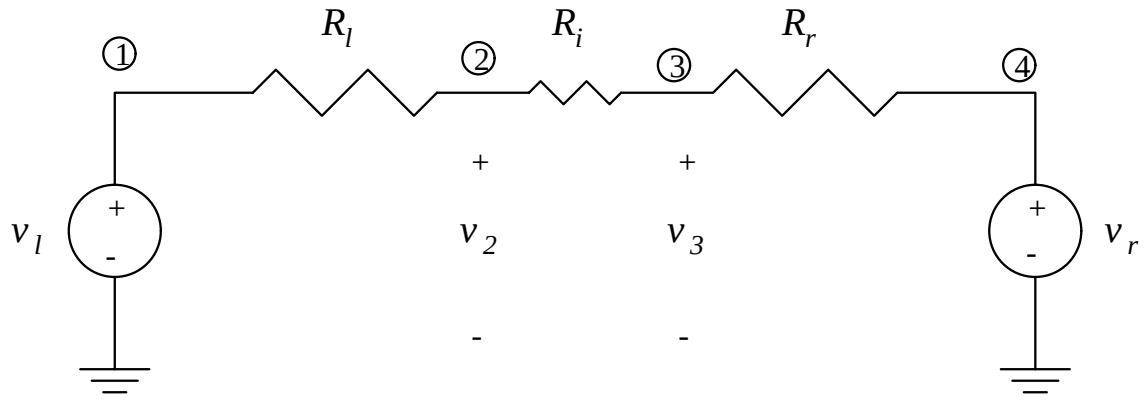

Figure 3-6: One-dimensional circuit model of spherical cell in steady-state.

The induced transmembrane potentials for the circuit model demonstrate the same properties described above for the spherical cell body model. Define

$$v_{ml} = v_2 - v_l = \frac{R_l}{R_l + R_i + R_r}(v_r - v_l),$$

$$v_{mr} = v_3 - v_r = \frac{R_r}{R_l + R_i + R_r}(v_l - v_r),$$

where v_{ml} is the potential induced across the left membrane resistance, and v_{mr} is the potential induced across the right membrane resistance. First, observe that hyperpolarizations occur at the side of the greater extracellular voltage, and depolarizations occur at the side of the smaller extracellular voltage. If $v_l > v_r$, for instance, the induced potential will be negative across the left membrane resistance, corresponding to a hyperpolarization, and positive across the right membrane resistance, corresponding to a depolarization. This property, which is analogous to the cosine proportionality of V_m above, is illustrated with voltage profile plot similar to that of Figure 3-5. A discretized version of the plot may be produced if the distance variable z is replaced with node numbers. The plot in Figure 3-7 was produced in this manner with $R_l = R_r = 10^{11}\Omega$, $R_i = 4{\times}10^7\Omega$, and $v_r = -v_l = 1.5mV$. These values were chosen so that induced voltages would be comparable to those of the three dimensional model along its z-axis: R_i is the resistance of a cylindrical "core" of conductivity σ_i (see Table 3.2), cross-sectional area $1\mu m^2$ and length $20\mu m$; R_l and R_r are the resistances of a $1\mu m^2$ area patch of membrane; and v_r and v_l are the extracellular voltages at $z = \pm R$, respectively, in Figure 3-5. As before, the dashed vertical lines represent the cell membrane.

Second, the transmembrane potentials induced in the 1-d circuit model decrease with decreasing membrane resistance. The analogous property for cell body model is that $V_m \downarrow 0$ as $G_m \uparrow \infty$. As R_l and R_r become comparable to R_i, the voltage drops over the three resistances become comparable. If the voltage drop $v_l - v_r$ were unchanged, the jumps in potential across the cell membrane resistances would decrease. We have stated above, however, that a change in cell model properties can result in a change in the extracellular voltages created by an extracellular electrode. Consider figure 3-8a, which was created by increasing G_m by a factor of 10,000. The extracellular voltage at $z = R$ has dropped

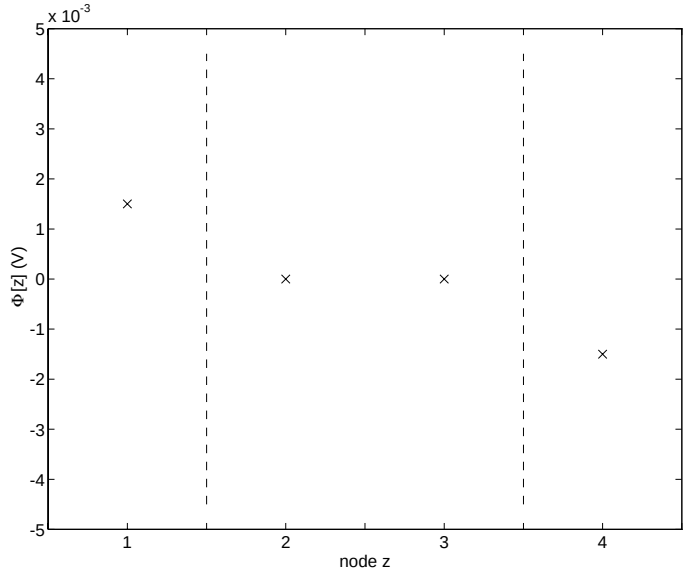

Figure 3-7: Voltage profile for circuit model of cell body.

slightly to 1.38mV. Thus, increasing the membrane conductance actually shrinks the induced transmembrane potentials in two ways: (1) by reducing the total voltage dropped across the cell model diameter; and (2) by causing an increased fraction of this voltage to be dropped across the intracellular resistance. A plot of node voltages for $R_l = R_r = 10^7\Omega$, $R_i = 4 \times 10^7\Omega$ and $v_r = -v_l = 1.38$mV is shown in Figure 3-8b to illustrate the effect of low membrane resistance in the circuit model.

Third, the transmembrane potentials induced in the circuit are proportional to the total voltage applied across it, $v_l - v_r$. This explains the remaining two properties. The total voltage established across the sphere is proportional to both the applied electric field E_o and the radius R. Thus, V_m is proportional to both of these quantities. Note that if the voltages v_l and v_r are equal, no depolarizations or hyperpolarizations will be created. The corresponding voltage profile will be entirely flat, since $v_2 = v_3 = v_l = v_r$ in such a case.

Generalization

The potential averaging property of the simple circuit model of Figure 3-6 may be generalized to an arbitrary number of conductances and voltage sources. This suggests a model such as that of Figure 3-9, where each conductance represents a differentially small patch of membrane and each voltage source represents the extracellular voltage at that patch. The intracellular resistances are assumed to have negligible effect on intracellular potential averaging, and are left out of the model. Comparison of Figures 3-5 and 3-8a suggest that this assumption is reasonable for the cell body model. The model may be used for an arbitrarily shaped cell provided that such intracellular resistances are small.

If G_j is the conductance of patch j and V_j is the extracellular potential, as labeled, we have

$$V_{mj} = \frac{\sum_{i=1}^{n} G_i(V_i - V_j)}{\sum_{i=1}^{n} G_i}$$

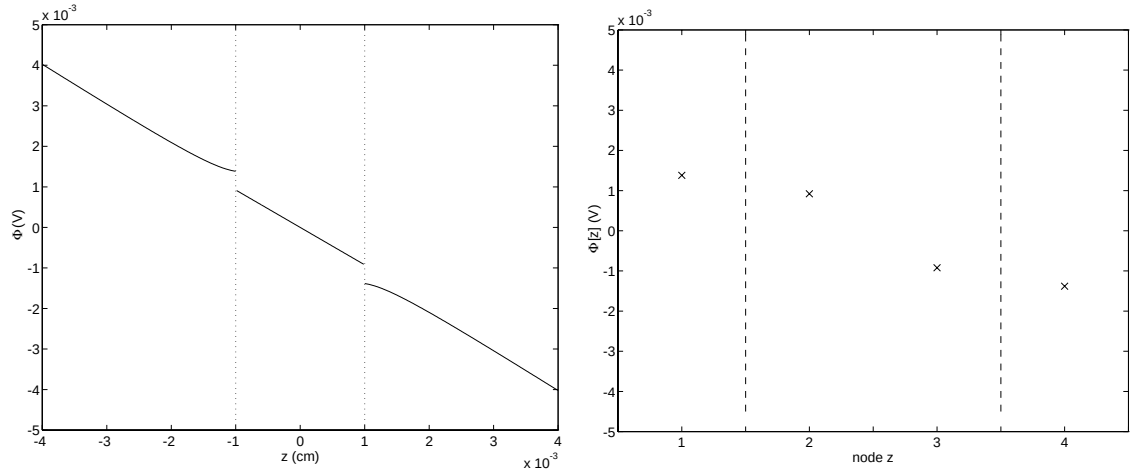

(a) (b)

Figure 3-8: Voltage profiles for (a) spherical cell body model with membrane conductance increased 10000-fold; (b) circuit model with R_l and R_r comparable to R_i.

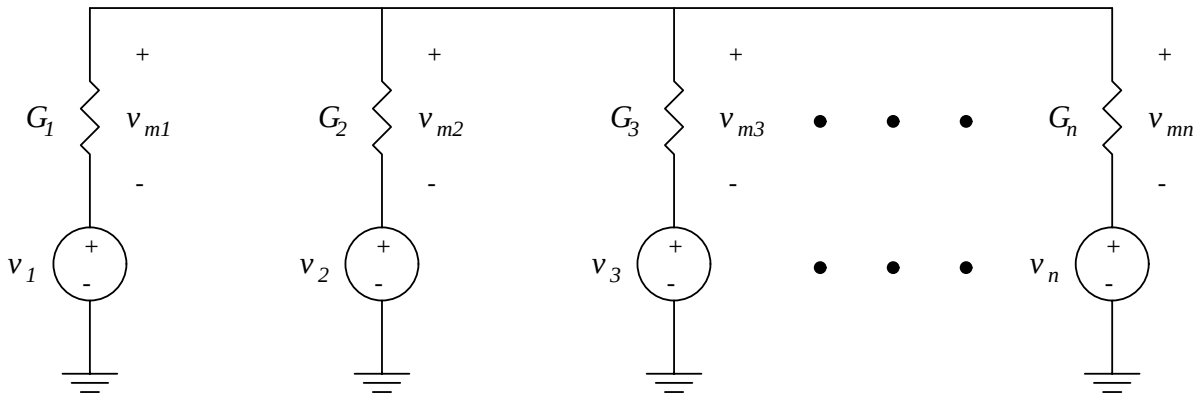

Figure 3-9: Circuit model for cell with small intracellular resistance in steady-state.

for the induced transmembrane potential. Note that V_{mj} will be small in areas where G_m is relatively large. This is because at patch j, G_j appears in the denominator of V_{mj}, which it dominates (by assumption), but is multiplied by zero in the numerator. This result has two important implications. First, for cells with spatially nonuniform membrane conductances, smaller transmembrane potentials will be induced in areas of higher conductance. Second, if the extracellular potentials are near some voltage V_j over a significant fraction of the cell's area, the induced transmembrane potentials will tend to be small in those areas. In this case, the total conductance path associated with V_j will appear large, since it represents a parallel combination of several patch conductances.

This second phenomenon may occur when a cell body stimulated with a point electrode, as in Figure 3-10. The electrode has a needle-like tip which is connected to the negative terminal of a current source. The return path for the current is assumed to be very far away. A potential profile characterized by a sharp, localized drop under the electrode tip is created in the extracellular space, as drawn in the trace labeled V_e in the lower portion of the Figure. Assume this potential drop occurs within a distance comparable to or smaller than the diameter of a cell body. Qualitatively speaking, the extracellular potentials in the vicinity of the electrode will vary more rapidly in the horizontal direction (as drawn) than in the vertical direction. In such a case, the vertical walls of the cell (emphasized with dotted lines in the Figure) will be at roughly the same extracellular potential. Remembering that the cell is a three-dimensional structure, it is clear that the side walls of the cell constitute a dominant fraction of its surface area. Thus the extracellular potential at these regions sees a large membrane conductance. For this reason, the induced intracellular potential profile (dotted line trace in Figure 3-10) will average out to a value which is close to the extracellular potential near the side walls of the cell. On the other hand, the membrane area directly beneath the electrode constitutes a small fraction of the cell's surface area, and thus represents a small conductance. The induced intracellular potential in this region will average out to a value which is relatively far from the local extracellular potential. Since the induced intracellular potential is much greater than the extracellular potential, this area of membrane is strongly depolarized by the point electrode. The actual intracellular voltage is found by adding the induced intracellular potentials to the rest potential V_r, yielding the V_i trace.

Small changes in intracellular potential occur due to intracellular resistances. Since in cell bodies these resistances act over short distances and more or less in parallel, they do not significantly affect the potential profiles. By contrast, intracellular resistances in axons occur over long distances and in series. As we will see in the next section, this dramatically alters the way extracellular voltages induce transmembrane potentials.

3.3 Axon in a longitudinal field

For applied electric fields with components longitudinal to an axon, it is useful to examine the cable model shown in Figure 3-11. The axon model is assumed to be of (doubly) infinite length. The axonal membrane is represented as a distributed series of resistances and capacitances in parallel, separated at the interior of the cell by an axial resistance. There are many variables associated with this model, which are listed in Table 3.3 for reference. The variable meanings are also illustrated in the circuit diagram of Figure 3-12. All currents and potentials are assumed to be radially symmetric, and all currents flowing through the membrane are assumed to flow in a radial direction only. Note that several

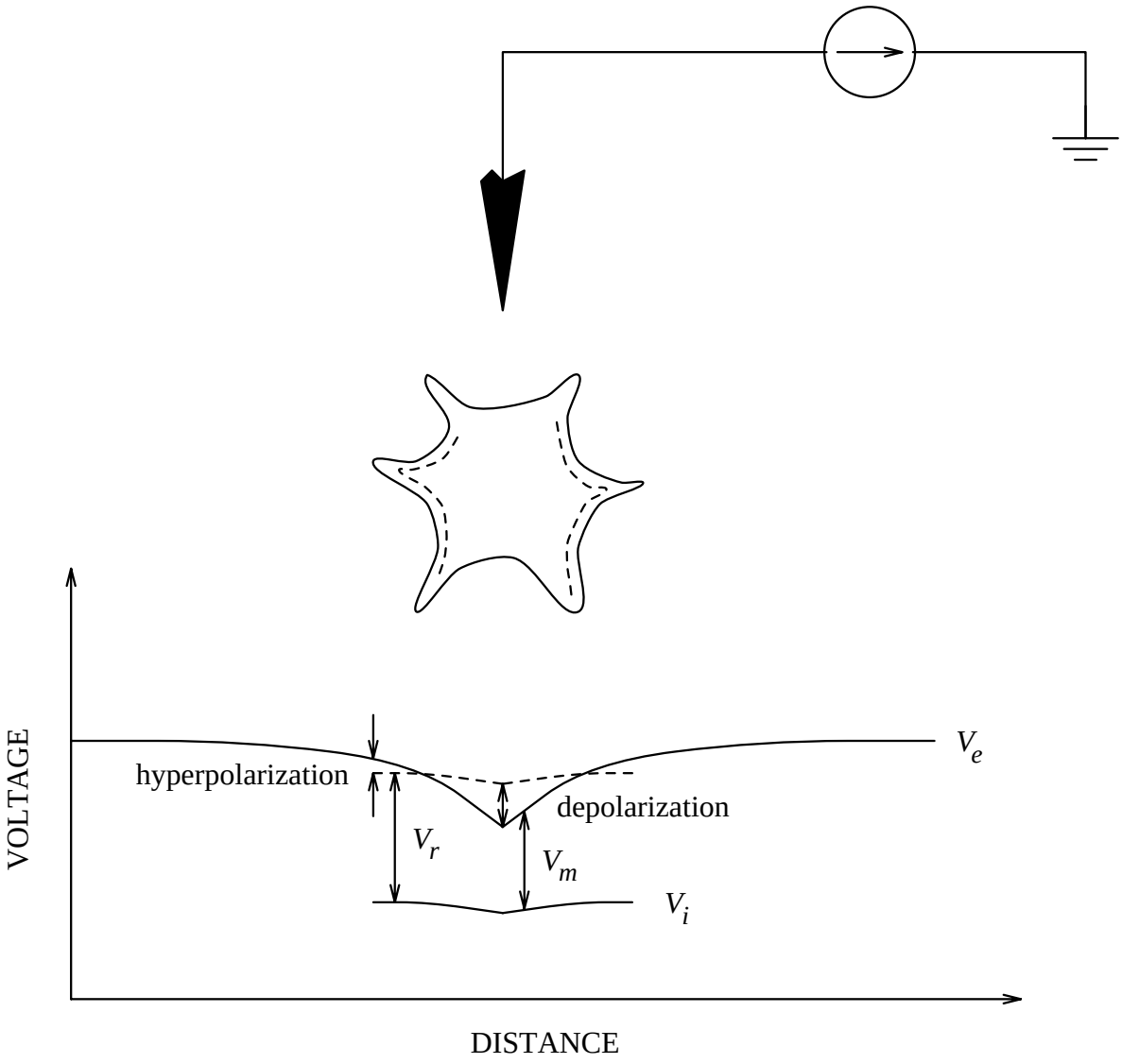

Figure 3-10: Schematic of point electrode stimulation.

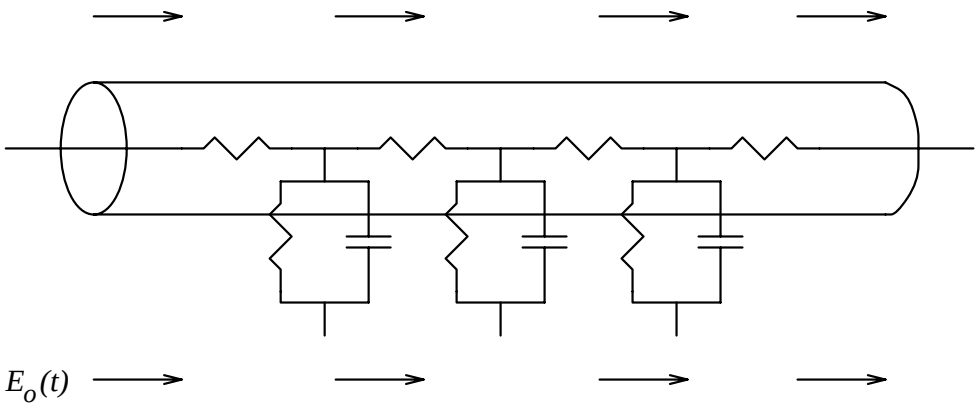

Figure 3-11: Schematic of axon in a longitudinal field.

Variable	Name	SI Unit
$V_m(z,t)$	Transmembrane potential	Volts
$V_i(z,t)$	Intracellular potential	Volts
$V_e(z,t)$	Extracellular potential	Volts
$I_i(z,t)$	Intracellular axial current	Amperes
$k_m(z,t)$	Membrane current per unit length	Amperes/meter
r_i	Intracellular resistance per unit length	Ohms/meter
g_m	Membrane conductance per unit length	Siemens/meter
c_m	Membrane capacitance per unit length	Farads/meter
λ_c	Space constant	meters
τ_m	Time constant	seconds
z	Length variable	meters

Table 3.3: Cable model variables defined.

of the variable expressions are multiplied by Δz. Since these variables are given in "per unit length" units, multiplication by some length is necessary to give the circuit element or current the correct units. Note also that no assumptions about the extracellular medium were made to arrive at the circuit model; the voltages at the extracellular nodes are strictly set by $V_e(z,t)$. To determine the actual values of $V_e(z,t)$, on the other hand, one must know the stimulating electrode configuration, the stimulus waveform and amplitude, the electrical properties of the extracellular medium, and the electrical properties of the axon. Even with such knowledge, however, an analytical solution for $V_e(z,t)$ is not guaranteed. Therefore, following a few initial derivations and remarks, a simple time-independent extracellular voltage will be assumed (see Figure 3-14a).

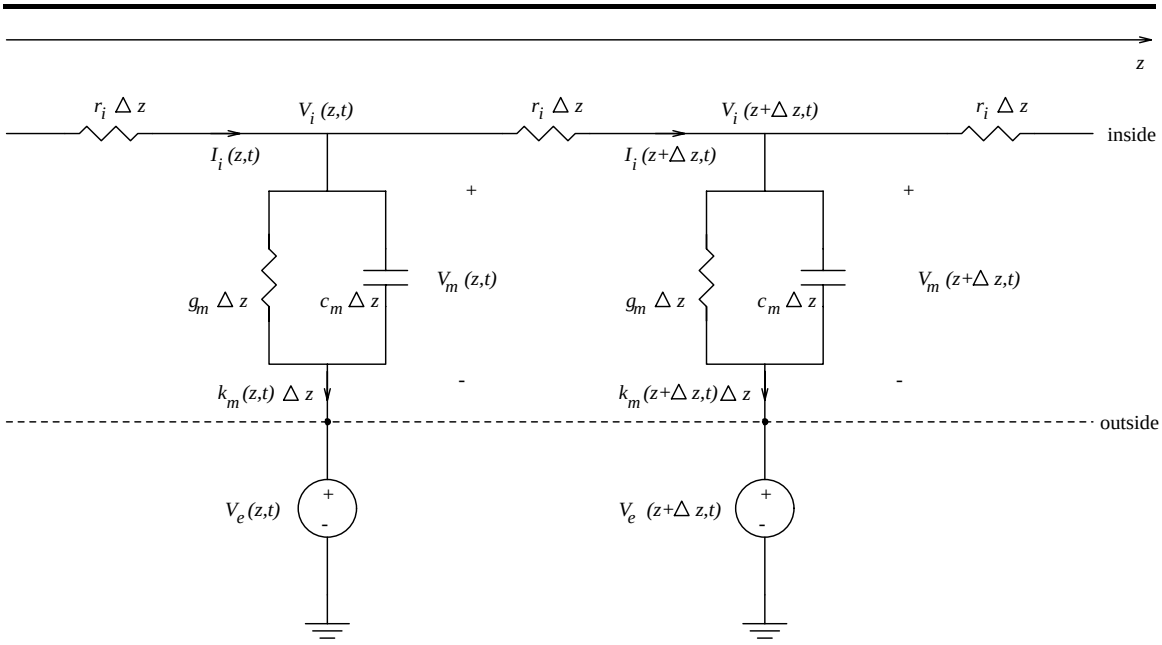

Figure 3-12: Cable model variables illustrated.

3.3.1 Cable equation for extracellular stimulation

Using Kirchoff's Current and Voltage Laws, three equations can be written for the circuit of Figure 3-12 which, in the limit where Δz approaches zero, become

$$\frac{\partial V_i(z,t)}{\partial z} = -I_i(z,t)r_i, \tag{3.16}$$

$$\frac{\partial I_i(z,t)}{\partial z} = -k_m(z,t), \tag{3.17}$$

$$k_m(z,t) = c_m\frac{\partial V_m(z,t)}{\partial t} + g_m V_m(z,t). \tag{3.18}$$

Equations (3.16)-(3.18) can be combined to form a single equation,

$$-\lambda_c^2\frac{\partial^2 V_i(z,t)}{\partial z^2} + \tau_m\frac{\partial V_m(z,t)}{\partial t} + V_m(z,t) = 0, \tag{3.19}$$

where

$$\lambda_c = \sqrt{\frac{1}{g_m r_i}} \tag{3.20}$$

is the length constant of the axon, and

$$\tau_m = \frac{c_m}{g_m} \tag{3.21}$$

is the time constant. Now, noting that

$$V_m(z,t) = V_i(z,t) - V_e(z,t) \tag{3.22}$$

and that the second partial derivative operator is linear, add $\lambda_c^2 \frac{\partial^2 V_e(z,t)}{\partial z^2}$ to both sides of equation (3.19) to obtain

$$-\lambda_c^2 \frac{\partial^2 V_m(z,t)}{\partial z^2} + \tau_m \frac{\partial V_m(z,t)}{\partial t} + V_m(z,t) = \lambda_c^2 \frac{\partial^2 V_e(z,t)}{\partial z^2}. \tag{3.23}$$

This partial differential equation in V_m provides a useful tool for the analysis of extracellularly applied electric fields. Rubinstein and Spelman used a similar equation to calculate the response of V_m to a two-dimensional impulse $V_e(z,t)$ using transform methods[52]. This impulse response may be convolved both in space and time to determine the circuit model response to an arbitrary extracellular potential distribution.

3.3.2 Activating function

Equation (3.23) suggests that V_e itself is not the fundamentally important quantity for inducing transmembrane potentials in the axon model. Rather, the second spatial derivative of the extracellular potential can be thought of as the "drive term". For this reason, the function was dubbed the *activating function* by Rattay[48]. Define the activating function

$$f_a(z,t) = \frac{\partial^2 V_e(z,t)}{\partial z^2} \tag{3.24}$$

and substitute into the previous result to obtain

$$-\lambda_c^2 \frac{\partial^2 V_m(z,t)}{\partial z^2} + \tau_m \frac{\partial V_m(z,t)}{\partial t} + V_m(z,t) = \lambda_c^2 f_a(z,t). \tag{3.25}$$

The activating function has important implications for extracellular electrical stimulation. If the applied extracellular potential depends on z and t only, then by the definition of the electric potential we have

$$E_o(z,t) = -\partial V_e(z,t)/\partial z$$

for the applied electric field. Taking a partial derivative in z on both sides of the above relation and using the definition of activating function, we have

$$f_a = -\partial E_o(z,t)/\partial z.$$

This means that the extracellular electric field must have a nonzero first derivative in the axon's longitudinal direction in order to induce transmembrane potentials. In contrast, recall from section 3.2 that only a spatially constant electric field was required to induce transmembrane potentials in the cell body model.

This fundamental difference in mode of activation can be explained on the basis of geometrical considerations. First, consider the cell body model. Since the spherically shaped intracellular fluid resembles a collection of short-length resistors in parallel with one another, its lumped intracellular resistance is small. Furthermore, the inside of the cell model is at a roughly constant potential due to the low intracellular resistance. Because the intracellular potential is constrained to be constant, transmembrane potentials will be induced at some points on the model if its external surface is not equipotential. Finally, a uniform electric field is sufficient to create a non-uniform extracellular potential distribution. Now consider the axon model geometry. The intracellular fluid resembles a long, *series* connection of

resistors. For this reason, intracellular resistances in the axon model are substantial. If just the right amount of current is flowing inside of the axon, the intracellular potentials can track the linearly varying extracellular potentials created by a constant electric field. Thus, a spatially constant extracellular electric field is not sufficient to induce transmembrane potentials in the axon model. Of course, current must flow into and out of the axon model at some locations; transmembrane potentials are necessarily induced at these locations. If the axon model is of infinite length - the case that is examined in this thesis - transmembrane current flow will only occur in or near regions where the extracellular electric field has a nonzero first spatial derivative (see, for example, Figure 3-16). If the axon model is of finite length, transmembrane currents might flow through the ends of the model.

The response of V_m may be found for the two-dimensional (in z and t) impulse activating function and convolved to find V_m for an arbitrary f_a. Since we are concerned with the steady-state case in this thesis, however, only the time-independent impulse response will be derived.

3.3.3 Time-independent solutions

In cases where the applied electric field is not changing with time and all transients have died out, equation (3.25) reduces to

$$-\lambda_c^2 \frac{d^2 V_m(z)}{dz^2} + V_m(z) = \lambda_c^2 f_a(z). \tag{3.26}$$

Solutions of this time-independent cable equation may be found for an arbitrary extracellular electrode configuration if we obtain its impulse response. Let the activation function be a spatial impulse in z,

$$f_a(z) = E_o \delta(z). \tag{3.27}$$

First solve the homogeneous equation

$$-\lambda_c^2 \frac{d^2 \hat{V}_m}{dz^2} + \hat{V}_m = 0,$$

where the "hat" notation has been introduced to denote the impulse response of the induced transmembrane potential. This equation can be solved using standard techniques for ordinary differential equations with constant coefficients. Let

$$\hat{V}_m = A e^{pz}.$$

Substituting this expression into the homogeneous equation and solving for p, we find that

$$p = \pm \frac{1}{\lambda_c}.$$

Solutions of this form apply in regions where the drive is zero, i.e. on either side of the V_m axis, so

$$\hat{V}_m = \begin{cases} A_1 e^{-z/\lambda_c} + A_3 e^{z/\lambda_c} & \text{for } z > 0, \\ A_2 e^{z/\lambda_c} + A_4 e^{-z/\lambda_c} & \text{for } z < 0. \end{cases}$$

Since the axon model is infinitely long, on physical grounds we expect the transmembrane potential to decay to zero far away from the stimulus. A_3 and A_4 must then be zero, leaving

$$\hat{V}_m = \begin{cases} A_1 e^{-z/\lambda_c} & \text{for } z > 0, \\ A_2 e^{z/\lambda_c} & \text{for } z < 0. \end{cases}$$

It will now be shown that $\hat{V}_m$ must be continuous at the origin. Suppose the opposite is true, implying that $A_1 \neq A_2$. The first spatial derivative of the transmembrane potential will contain an impulse, and the second spatial derivative will contain a doublet. On the other hand, substituting the drive term, equation (3.27), into the time-independent equation yields

$$-\lambda_c^2 \frac{d^2 \hat{V}_m}{dz^2} + \hat{V}_m = \lambda_c^2 E_o \delta(z).$$

Since this equation contains no doublets, $\hat{V}_m$ must be continuous at the origin. Letting $A_1 = A_2 = A$, we have

$$\hat{V}_m = A e^{-|z|/\lambda_c}.$$

The coefficient A can be found by the impulse matching argument illustrated in Figure 3-13 and is

$$A = \frac{\lambda_c E_o}{2}.$$

Finally, the transmembrane potential created by a spatial impulse activating function is

$$\hat{V}_m = \frac{\lambda_c E_o}{2} e^{-|z|/\lambda_c}. \tag{3.28}$$

3.3.4 Interpretation of the time-independent solutions

Recall the stimulus paradigm illustrated in Figure 3-2b. In order to determine the transmembrane potentials induced in the axon model by the parallel plates, it will be necessary to find the associated activating function. Consider the profiles plotted in Figure 3-14. Neglecting both fringing and also the influence of the axon model on the extracellular voltage, current will pass between the plates uniformly in the horizontal direction. Extracellular voltages will be constant outside of the plates where no current is flowing, and decrease linearly with z between the plates at $z = -d/2$ and $z = d/2$, as drawn in Figure 3-14a. The corresponding electric field profile is drawn in Figure 3-14b, and the activating function in Figure 3-14c. The activating function is simply two impulses of equal area E_o and opposite magnitude. Since the circuit model for the longitudinal axon is linear and time-invariant, we can find the total response of the induced transmembrane potential for this activating function by superposing two impulse responses of opposite magnitude and separated by a distance d. Thus

$$\boxed{V_m(z) = \frac{E_o \lambda_c}{2}(-e^{-|z+\frac{d}{2}|/\lambda_c} + e^{-|z-\frac{d}{2}|/\lambda_c}).} \tag{3.29}$$

It is clear from the plot of Figure 3-15a that, if $d \gg \lambda_c$, the individual impulse responses at $z = -d/2$ and $z = d/2$ appear distinctly. The point of maximal depolarization - the physiologically significant feature - occurs at $z = d/2$. As d is decreased, the individual impulse responses tend to cancel each other out as shown in Figure 3-15b. The total amount of maximal depolarization decreases, but still occurs at $z = d/2$. The value of this

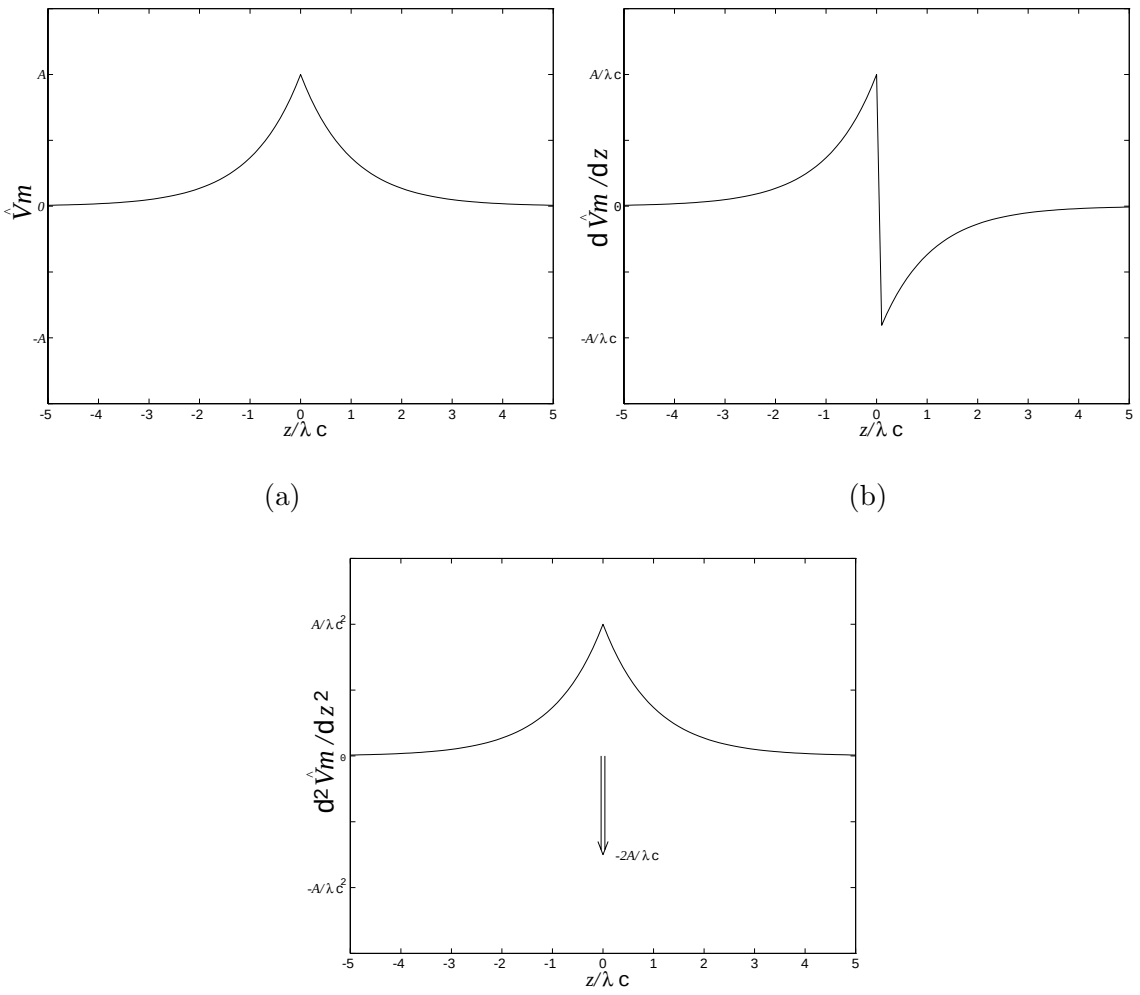

(a) (b)

(c)

Figure 3-13: Impulse matching to solve the time-independent cable equation for extracellular stimuli. The area of the impulse in plot (c) must be equal to $-E_o$.

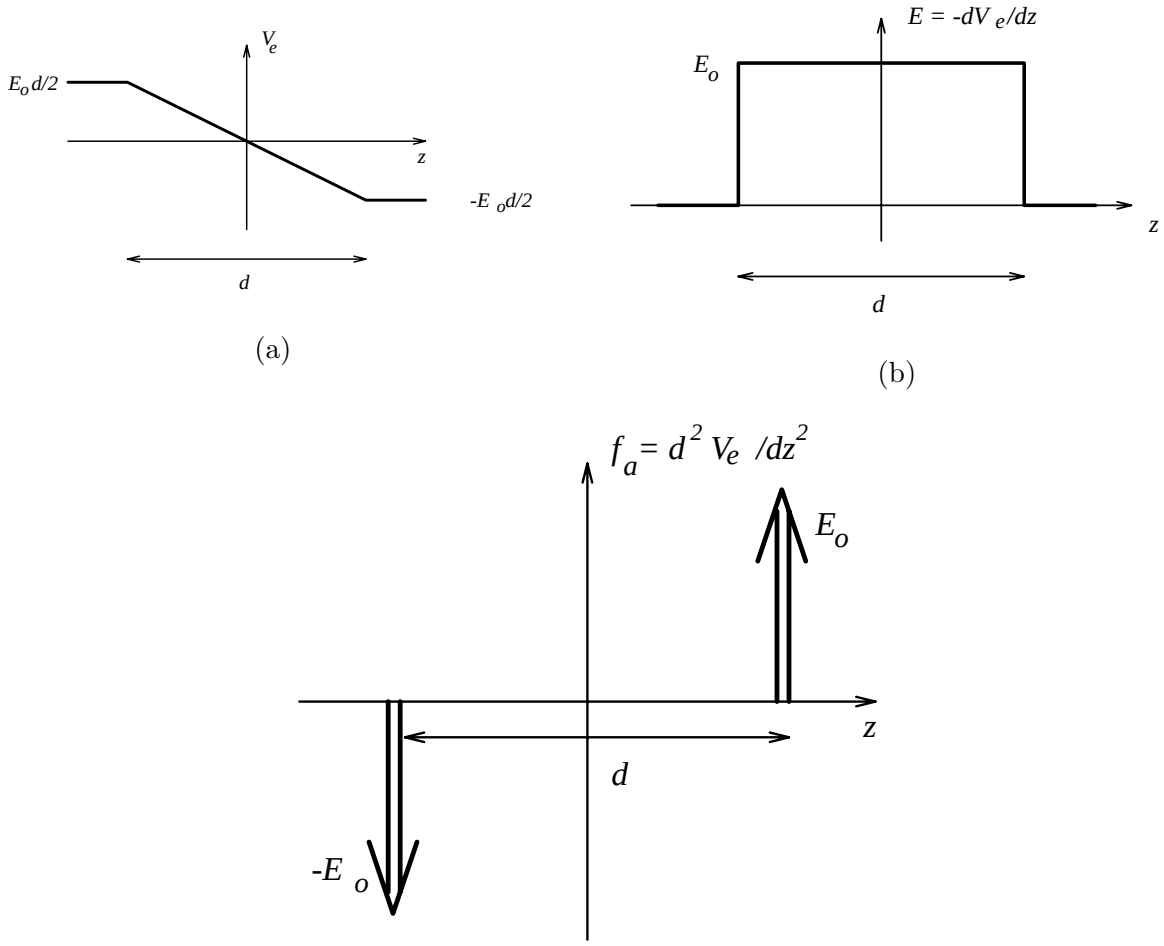

Figure 3-14: Profiles created by parallel plates with spacing d of (a) Extracellular voltage; (b) Extracellular electric field; and (c) Activating function

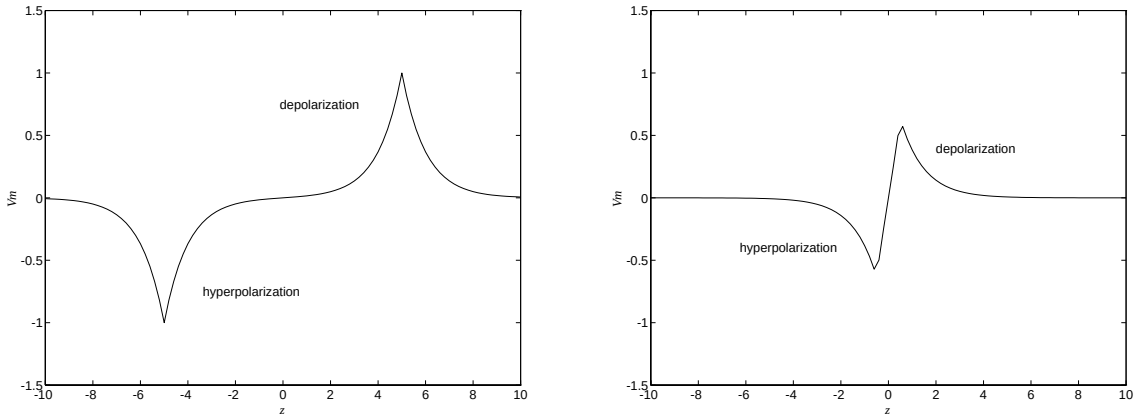

(a) (b)

Figure 3-15: Transmembrane potential profiles for plate spacing (a) $d = 10\lambda_c$; (b) $d = \lambda_c$. $E_o = 2$ and $\lambda_c = 1$ were used to produce plots.

depolarization is given by

$$V_m|_{z=d/2} = \frac{E_o \lambda_c}{2}(1 - e^{-d/\lambda_c}). \tag{3.30}$$

Note that the depolarization is maximal when d is infinitely large and decreases to zero as d goes to zero. In addition, the above relation allows us to predict the amount of electric field needed to produce a depolarization $V_{m,o}$:

$$E_o = \frac{2V_{m,o}}{\lambda_c}/(1 - e^{-d/\lambda_c}). \tag{3.31}$$

Potential averaging property

As in the case of the spherical cell body model, induced transmembrane potentials are the result of an averaging process. To see this, let $h(z)$ be the transmembrane potential induced by an impulse of extracellular voltage $V_e = \delta(z)$. This response is found by taking the second spatial derivative of equation (3.28) and neglecting the coefficient E_o, yielding

$$h(z) = \frac{1}{2\lambda_c} e^{-|z|/\lambda_c} - \delta(z).$$

Now note that the induced transmembrane voltage for arbitrary extracellular voltages may be found from the convolution integral

$$V_m(z) = \int_{-\infty}^{\infty} V_e(\xi) h(z - \xi) d\xi.$$

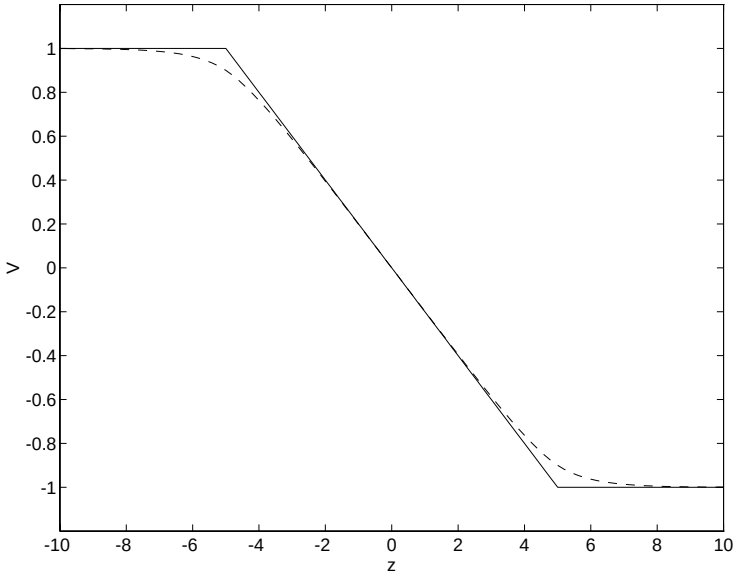

Figure 3-16: Extracellular (solid line) and intracellular (dashed line) voltages for parallel plate electrode with $\lambda_c = 1$, $d = 10\lambda_c$, and $E_o d = 2$. Intracellular potentials are found by adding the extracellular potentials to V_m.

Substituting the impulse response into the convolution integral yields

$$V_m(z) = \int_{-\infty}^{\infty} \frac{V_e(\xi)}{2\lambda_c} e^{-|z-\xi|/\lambda_c} d\xi - V_e(z).$$

And, finally, substituting equation (3.22) for V_m, we have

$$V_i(z) = \int_{-\infty}^{\infty} \frac{V_e(\xi)}{2\lambda_c} e^{-|z-\xi|/\lambda_c} d\xi. \tag{3.32}$$

Inspection of equation (3.32) reveals that the intracellular voltage at some location z along the axon consists of a weighted sum of the extracellular potentials. Furthermore, the weighting function is greatest at the "observation point" z, decreases monotonically and symmetrically as you move away from z, and has area 1. The potential averaging process implied by equation (3.32) is illustrated in Figure 3-16. The intracellular and extracellular potentials differ only near breakpoints ($|z| \approx 5$) where the extracellular potential is not the average of its neighboring values.

3.4 Comparison of thresholds

In the previous two sections, linear models were used to obtain closed-form solutions for the induced transmembrane potential. By assumption (see section 3.1), these models are valid only when the transmembrane potential is below some fixed threshold. Let this threshold be denoted by $V_{m,th}$, and assume that it is the maximum depolarization produced when an electric field E_{th} is established between the electrode plates. Suppose also that the

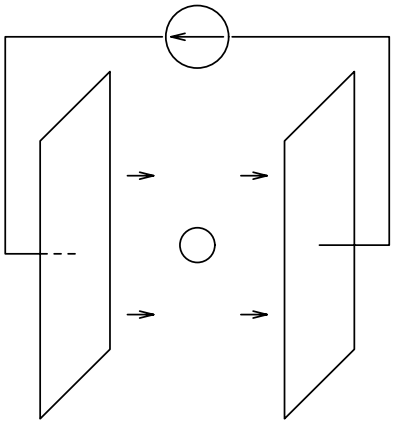

$$V_m = \frac{3\sigma_i\sigma_e R}{\sigma_i G_m R + 2\sigma_e G_m R + 2\sigma_i\sigma_e} E_o \cos\theta$$

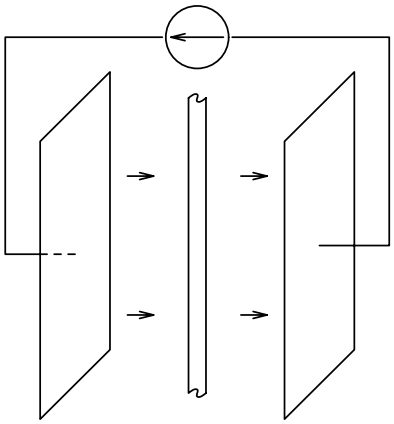

$$V_m = \frac{2\sigma_i\sigma_e R}{\sigma_i G_m R + \sigma_e G_m R + \sigma_i\sigma_e} E_o \cos\phi$$

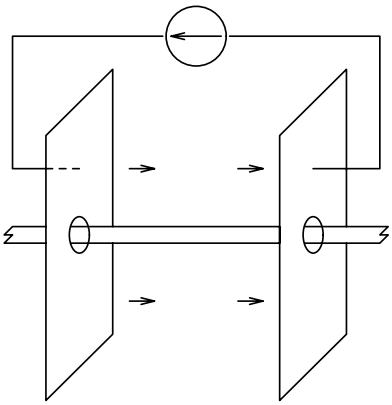

$$V_m(z) = \frac{E_o\lambda_c}{2}(-e^{-|z+\frac{d}{2}|/\lambda_c} + e^{-|z-\frac{d}{2}|/\lambda_c})$$

Figure 3-17: Summary of analytical derivations; transmembrane potentials for cell body in a uniform electric field (top), axon in a uniform, transverse field (middle) and axon in a longitudinal field (bottom).

maximal depolarization produced by an electric field E_o is denoted $V_{m,max}$. Express these relationships as

$$E_{th} \longrightarrow V_{m,th},$$

$$E_o \longrightarrow V_{m,max}.$$

Without loss of generality, we can write

$$V_{m,max} = kV_{th},$$

where k is an arbitrary real number. Thus, to produce the threshold depolarization, we wish to find the stimulus which yields $V_{th} = V_{m,max}/k$. Since our models are linear, we have

$$\frac{E_o}{k} \longrightarrow \frac{V_{m,max}}{k} = V_{th}.$$

Substituting for k in this last result, we have

$$E_{th} = \frac{V_{th}}{V_{m,max}} E_o. \tag{3.33}$$

From equation (3.33), we see that *the threshold electric field is inversely proportional to the maximum depolarization induced in the linear models by a (fixed) stimulating field* E_o. This fact will now be used to compare the thresholds for generating action potentials using the three stimulus paradigms of Figure 3-2.

A summary of the steady-state induced transmembrane potentials for the stimulus paradigms is provided by Figure 3-17. As discussed at the beginning of this chapter, the derivation and interpretation of the transmembrane potentials induced in an axon model by a uniform, transverse field are quite similar to those for the spherical cell body model. This analysis was therefore left out of the chapter, and may be found in Appendix A.2.

Using an axon radius of $R_a = 0.5\mu$m[26][4], a cell body radius of $R_{cb} = 10\mu$m[26] and the electrical parameters listed in Table 3.2, it can be shown that

$$V_{mcb} \approx 1.5 R_{cb} E_o \cos\theta,$$

$$V_{mta} \approx 2 R_a E_o \cos\phi,$$

where the subscript *cb* refers to the cell body and the subscript *ta* refers to the axon in a transverse field. Now consider the maximum levels of depolarization induced in the three models by the parallel plate electrode. For the cell body model, this occurs at $\theta = 0$, for the axon in the transverse field at $\phi = 0$, and for the axon in the longitudinal field at $z = d/2$. The maximum depolarizations are given by

$$V_{mcb,max} = 1.5 R_{cb} E_o,$$

$$V_{mta,max} = 2 R_a E_o,$$

$$V_{mla,max} = \frac{E_o \lambda_c}{2},$$

where the last formula applies for the case where d is much larger than the space constant.

[4]Radius of a rabbit retinal ganglion cell axon. See footnote 3.

Cell body vs. axon in transverse field

Taking the ratio of maximal depolarizations of the cell body and the axon in a transverse field yields

$$\frac{V_{mcb,max}}{V_{mta,max}} = 0.75 R_{cb}/R_a = 15.$$

Thus, the relative amount of transmembrane potential induced in the two models by the uniform electric field is proportional to the ratio of cell body radius to axonal radius. Using the radii given above, this ratio of depolarizations turns out to be 15. This result is qualitatively consistent with the discussion of section 3.2.3, where it was concluded that the total amount of polarization created in a cell body model was proportional to its radius. In light of equation (3.33), the threshold for stimulating axons with a transverse field will be 15 times higher than that for stimulating cell bodies.

Axon in longitudinal field vs. axon in transverse field

In general, an extracellular electric field will have components longitudinal to an axon as well as transverse to it. We can compare the relative effects of the two electric field components by taking the ratio

$$\frac{V_{mla,max}}{V_{mta,max}} = \lambda_c/4R_a \approx 56.$$

To determine this ratio numerically it will be necessary to determine the length constant λ_c of the axon model. This may be found from the definition given by equation (3.20) and by noting that $g_m \approx G_m(2\pi R_a)$ and $r_i = 1/\sigma_i \pi R_a^2$.

$$\lambda_c = \sqrt{\frac{\sigma_i R_a}{2G_m}}.$$

Using the numbers in Table 3.2, λ_c is calculated to be about 112μm. Plugging in the values for the axonal radius and length constant yields a depolarization ratio of about 56. The threshold for stimulating axons with a transverse field will therefore be 56 times higher than that for stimulating the axon with a longitudinal field.

An important distinction must be made when considering this comparison, however. Only a spatially constant electric field E_o is required to induce depolarizations in the axon when the field is applied transversely to it. By contrast, spatial gradients in E_o are necessary to induce transmembrane potentials when the field is longitudinal to the axon. To put it precisely, the ratio computed above is a comparison of the depolarization created by a uniform, transverse electric field and that created by a *step* in electric field of equal magnitude in a direction longitudinal to the axon.

Is this a reasonable comparison to make? I believe so for two reasons. First, consider the vast difference between the radius $R \approx 0.5\mu$m of an axon and the length constant $\lambda_c \approx 112\mu$m. A transversely applied field may be considered uniform if it does not change significantly within several radii of the axon, whereas a longitudinally applied field may be considered uniform if it does not change significantly over the course of several length constants. Since $\lambda_c \gg R$, spatial gradients in electric field will more likely be of consequence in the longitudinal direction than in the transverse direction. Second, the comparison may simply be viewed as that between two stimulus paradigms. The ratio computed above is simply an expression of the relative effects of the same electrode configuration in two

different orientations.

Axon in longitudinal field vs. cell body

The depolarizations created in the cell body model and the axon model in a longitudinal field may be compared by taking the ratio of the previous two ratios,

$$\frac{V_{mla,max}}{V_{mcb,max}} \approx 56/15 \approx 4.$$

Thus the parallel plate electrode is almost four times more effective in depolarizing the axon model than the cell body model. Furthermore, the threshold for stimulating cell bodies will be about four times that for stimulating axons with a longitudinal field.

3.5 Limitations of approach

A large number of assumptions were made to arrive at the analytical results of this chapter. To determine the quantitative effect that these assumptions will have on the derived results would be beyond the scope of this thesis. Instead, the purpose of the following section is to acknowledge the more critical of our assumptions and discuss their drawbacks.

3.5.1 Nonlinearity of the cell membrane

The consequences of ignoring active and nonlinear responses of nerve membranes were discussed in section 3.1. To recapitulate, passive and linear models fail to reproduce the familiar resting potential and action potentials. Linearizing the electrical properties of cell membranes about the rest potential permits the use of straightforward analytical techniques to determine the effects of extracellular electric fields. Analysis of this type reveals *how* and *where* membrane depolarizations and hyperpolarizations will be induced in cell body and axon models by an extracellular stimulus. In order to determine the relative excitability of cells in the three stimulus paradigms, it was assumed that the linear models were valid until a fixed threshold depolarization was reached. There are several indications that the threshold for extracellular stimulation may depend on the time pattern of the stimulus (see below). This may not be an issue if the stimuli used in the three paradigms have the same time pattern. On the other hand, linear models are only valid up until some fraction of the threshold.

3.5.2 Time-dependent behavior

In this chapter, only steady-state responses were examined. Experimental nerve preparations involve time-dependent stimuli (even a constant stimulus must be turned on at some point) and time-dependent cellular responses. How might the approach of this chapter be generalized to account for time-dependent behavior? If the linear approximation were valid up to some fixed threshold, a simple approach could be taken: calculate the time-dependent responses of the different models for a time-dependent electric field, and determine excitability based on how much time and field strength are needed to produce the threshold depolarization in each of the models. Does there exist a critical threshold depolarization at which action potentials are always produced? To answer this question, consider the phenomenon of accommodation and the strength-duration relation.

Accommodation

A step in applied current may cause a nerve cell to activate, while a slow ramp attaining the same final value of current does not[63]. Clearly, this accommodating behavior demonstrates that the time pattern of a stimulus is critical in determining whether or not a cell will be excited. Note that, for both "slow" and "fast" stimuli, the same amount of steady-state depolarization would be produced in a linear model of a cell. This suggests that the threshold for generating action potentials is dependent on the time pattern of the stimulus. On the other hand, it is well known that as threshold is approached, linear models of cells break down. If this were the case, the same steady-state applied current might not produce the same depolarization for the two types of stimuli.

Strength-duration relation

A common finding in electrophysiological experiments is that, when using a square pulse of current, the threshold strength required to elicit action potentials is a function of the pulse duration. Many strength-duration curves fit the empirical equation

$$I_{th} = I_r(1 + C/T)$$

, where I_{th} is the threshold current, I_r is the *rheobase* current, T is the pulse duration, and C is called *chronaxie*[46]. Note that for pulse durations which are small compared to the chronaxie $I_{th} \approx I_r C/T$. Thus there is a threshold charge $Q_{th} = I_{th}T = I_r C$ which is independent of T for small T. Suppose this charge is applied to the inside of a cell with lumped capacitance $C_M = 4\pi R^2 C_m$, as in Figure 3-18. A potential

$$V_{th} = Q_{th}/C_M$$

will be established across the membrane. Thus, for intracellular stimuli of short duration, the cell membrane demonstrates a fixed membrane potential at which action potentials will be generated. This fact is rigorously demonstrated by Weiss for the space-clamped Hodgkin-Huxley model of the squid axon[63]. Furthermore, the strength-duration is approximated over the entire range of durations with a parallel RC model of the cell membrane which charges up to a fixed threshold[63].

Unfortunately, interpreting the strength-duration relation is less straightforward for extracellular stimuli. In contrast to charge applied intracellularly to a cell body or space-clamped axon, extracellularly applied charge will not build up uniformly against cell membranes. As a consequence, lumped-parameter circuit models must be replaced with distributed models such as those used in the previous sections. The time constants of the linear models analyzed in this chapter are determined in appendices A.1,A.2.3 and B. These are summarized in Table 3.4. The time constants of the spherical cell model and axon in a transverse field are so small that such models reach steady-state within a microsecond. If the membranes generated action potentials at a fixed threshold V_{th} as hypothesized above, it would be difficult to explain changes in threshold for pulse durations much greater than a few microseconds with these models. This is not consistent with the fact that chronaxies determined in extracellular stimulation experiments are typically tens of microseconds or more[45]. The time constant for the model of the axon in a longitudinal field is substantially larger, and might in fact be consistent with the notion of a fixed threshold. McNeal numerically determined the strength-duration curve for a Frankenhauser-Huxley model frog

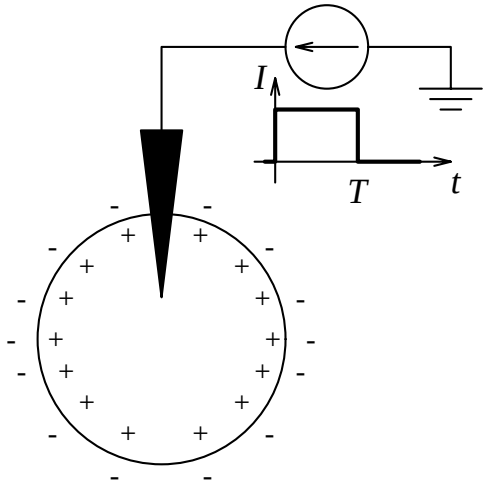

Figure 3-18: Intracellular stimulation with square pulses of current.

Model	Time constant
Cell body	225ns
Axon/transverse field	12.5ns
Axon/longitudinal field	0.4ms

Table 3.4: Time constants for different models.

myelinated nerve which was stimulated by a monopolar spherical electrode located 1mm away from one of the nodes. McNeal's calculations, however, fail to demonstrate a constant voltage threshold, even at pulse durations as low as 10μs. It is unclear whether this behavior is a property of the electrode configuration, the Frankenhauser-Huxley equations, or a combination of both.

In light of what is known about accommodation and the strength-duration relation, the threshold depolarization for generating action potentials appears to depend on the time pattern of the stimulus used.

3.5.3 Role of the cell in determining the extracellular voltage

In cases where circuit models were analyzed (see Figures 3-9 and 3-12) it was assumed that the extracellular voltage produced by the stimulating electrode was not deformed by the presence of the cell. It is clear, however, from the electroquasistatic models that this approximation is weakest in the region of greatest interest to the circuit models: immediately outside the cell. For example, the extracellular voltage in Figure 3-5 deviates maximally from a straight line at $|z| = R$.

3.5.4 Inhomogeneity of biological tissue

To determine the extracellular electric field produced by the parallel plate electrode, it was assumed that cells reside in a homogeneous extracellular medium. In general this is not the case. In the retina, for example, the extracellular space between its neural and glial cells is confined to gaps about 20nm wide (see chapter 2).

3.5.5 Anode-break excitation

A common phenomenon in electrophysiology occurs when a hyperpolarizing extracellular stimulus (an anode) is suddenly turned off[63]. Cells have been known to activate in some such cases, indicating that depolarizing a cell's membrane is not the only way to generate action potentials.

3.5.6 Non-uniformity of the cell membrane

It has been asserted that light evoked action potentials are initiated at the initial segment of amphibian retinal ganglion cell axons [7]. Studies yielding similar results for extracellular electrical stimulation of nerve cells have been cited by Ranck[46]. The existence of such "trigger zones" indicates that cell membranes may not have uniform electrical properties.

Chapter 4

Electrode Design

In this thesis we are interested in preferentially stimulating retinal ganglion cell bodies. Ideally, current delivered by our stimulating electrode will produce action potentials in cell bodies while evoking only passive responses from nearby axons. Thus in the ideal case the threshold for stimulating axons will be much higher than that for stimulating cell bodies.

Our design strategy is based on the assumption that the depolarization produced in the linear models is inversely related to the threshold for generating action potentials. It was found in chapter 3 that depolarizations could be induced in a spherical cell body model by a spatially uniform electric field. Due to the symmetry of the model, the orientation of the electric field is arbitrary. On the other hand, the depolarizations induced in the axon model depend strongly on the electric field orientation. A uniform electric field crossing the model in a transverse direction is sufficient to induce a depolarization, whereas a field parallel to the model must have a nonzero first derivative in that direction.

These results suggest that a stimulating electric field with carefully chosen spatial properties might provide some selectivity for cell bodies over axons. The spatial pattern of the electric field will be determined to a large extent by the geometry of the stimulating electrode. We therefore view the problem of selective stimulation as one of choosing the right electrode geometry.

This chapter is divided into three sections. The first section describes an electrode geometry which we believe will preferentially stimulate cell bodies. The second section provides the details of how the electrode was constructed. Finally, the third section discusses a model for predicting the electric field produced by the electrode.

4.1 Geometry

Consider the ideal parallel plate electrode analyzed in the previous chapter. Suppose a single axon model, oriented parallel to the plates, and a single cell body model reside between the plates of this electrode. If the cell body and axon models are far enough apart that they may be considered "in isolation", then the results of section 3.4 are applicable to this case. It was found in that section that the depolarization in each of the models is proportional to its size. Since the constants of proportionality are similar and ganglion cells are somewhat larger than axons, the amount of depolarization created in the cell body model is greater than that in the axon model. Furthermore, since the plates in this case are arbitrarily large, the applied electric field will have no component longitudinal to the axon model. Thus no additional depolarization will be created by longitudinal effects.

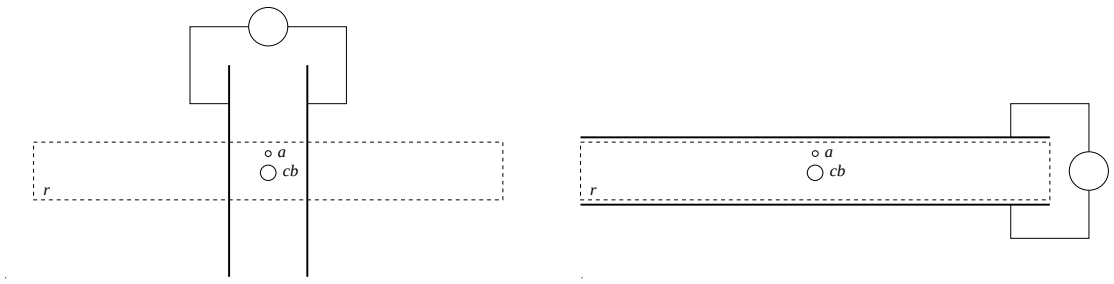

(a) (b)

Figure 4-1: Schematic of parallel plate electrode in two different orientations relative to the retina. (a) Plates oriented perpendicular to the retinal surface; (b) Plates oriented parallel to the retinal surface. Abbreviations: *r* - retina; *a* - axon; *cb* - cell body.

Figures 4-1a and 4-1b illustrate how we apply this reasoning to stimulation of retinal cells. In the Figure, large parallel plate electrodes are arranged in two different orientations relative to the retina. The axon, which projects perpendicular to the page in both cases, is parallel to the plates. Our (admittedly simplified) model posits the retina as a linear, isotropic, and homogeneous conductor. In addition, the cell body and axon models are assumed to be far enough apart to be considered in isolation. Under these assumptions and based on the comparison of section 3.4 above, we might expect to find lower thresholds for cell bodies than for axons with the parallel plate electrode.

Unfortunately, this electrode is impractical for use with a retinal implant. The orientation shown in Figure 4-1a is undesirable because it penetrates the retina, which would damage the tissue. The orientation in Figure 4-1b is undesirable because it places a plate on either side of the retina. By contrast, the implant's stimulating electrodes will all reside at the inner surface. Furthermore, due to their large size, both electrode configurations will influence the cells over vast regions of the retina. The implant, on the other hand, is to be used to stimulate cells in localized regions. Thus, alternatives to the electrode configurations of Figure 4-1 must be found.

One such alternative is to approximate the electrode of Figure 4-1a by using only its cross-section in the plane of the retina. This cross-section consists of two parallel, infinitely long wires. Limiting the length of the wires results in the electrode shown in Figure 4-2. If the wires' length is substantially larger their spacing, there will be regions of uniform electric field between the wires. By the reasoning presented above, this electrode might also be used to preferentially stimulate ganglion cells.

Some warnings must be made regarding the approximation of Figure 4-2. First, unlike the parallel plate electrode, the strength of electric field created by this electrode will decrease with distance from the retinal surface. Electric fields passing through nearby axons will be stronger than those passing through the more distant cell bodies. The applicability of the comparison of section 3.4 to the electrode of Figure 4-2 therefore depends on how rapidly the electric field decays with distance. Second, as suggested in the Figure, there will be fringing of the electric field around ends of wires. If all retinal axons were centered exactly between wires, fringe fields would cross the axons in a purely transverse direction.

However, in addition to the single axon drawn in the Figure, there are many other ganglion cell axons at the inner retinal surface. Fringe fields will produce longitudinal effects in axons which are closer to one or the other of the wires, perhaps increasing the total amount of depolarization created by the electrode. Thus, axons directly under the wires might be just as likely or even more likely to be stimulated than the cell bodies beneath them.

The disadvantages inherent in the parallel wire geometry are hard to quantify without a detailed knowledge of the electric field it produces. A model for predicting the field will be proposed in section 4.3. Electrodes were constructed in the absence of this knowledge, with the thought in mind that their ultimate effectiveness (or lack thereof) would be determined in experiments.

4.2 Construction

Electrodes with the geometry of Figure 4-2 were constructed by the author at MIT Lincoln Laboratory during the summer of 1993 and the month of January, 1994. Note that only the general shape of the electrode is indicated by the reasoning above. The additional variables of *materials* and *size* must be determined in order to completely specify the electrode. A number of factors including biocompatibility of materials, availability of materials, and various practical considerations influenced the final determination of these less conceptually important variables. Such factors will be discussed where appropriate in the outline of electrode construction presented below.

The stimulating electrodes used by the retinal implant will be created using photolithography techniques commonly employed in microelectronics fabrication. Using such techniques, arrays of electrodes having complex geometries can be routinely produced. It was decided, however, that the time and resources required for successful microfabrication made such electrodes impractical for this thesis. A more economical though less flexible method for producing single electrodes was employed. This method is illustrated step by step in the six panels of Figure 4-3. Each of these steps will now be described in detail:

1. **Cut a thin strip of conductor-insulator-conductor sandwich.** The starting material for the electrode was a square piece of fused silica which had been coated on either side with a 5μm thick layer of gold (MIC Technology, Richardson, TX). Coated substrates such as this are commonly patterned and used for high performance Hybrid Microwave Integrated Circuits. For our purposes, this conductor-insulator-conductor "sandwich" provided a convenient way to obtain the electrode geometry illustrated in Figure 4-2. The shaded square and rectangle in the upper part of Figure 4-3.1 represent a head-on view of the material, before and after a thin slice was cut along the dashed line with a wafer saw. The lower portion of Figure 4-3.1 is a cross-sectional view showing the insulator (white) sandwiched between the two conductors (shaded).

   The thickness of the fused silica in the conductor-insulator-conductor sandwich determined the electrode wire spacing (d in Figure 4-4b). This material was available in two thicknesses, one corresponding to a wire of spacing 127μm and the other yielding a spacing of 254μm. The length of the wires (l in Figure 4-4b) was equal to the width of the slice in Figure 4-3.1. Presumably, the greater the wires' length relative to their spacing, the better the uniform field approximation between the middle portions of the wires. Conductors could not be made arbitrarily long, however, because relatively small electrode tips were required for experiments (see Chapter 5). Slices of

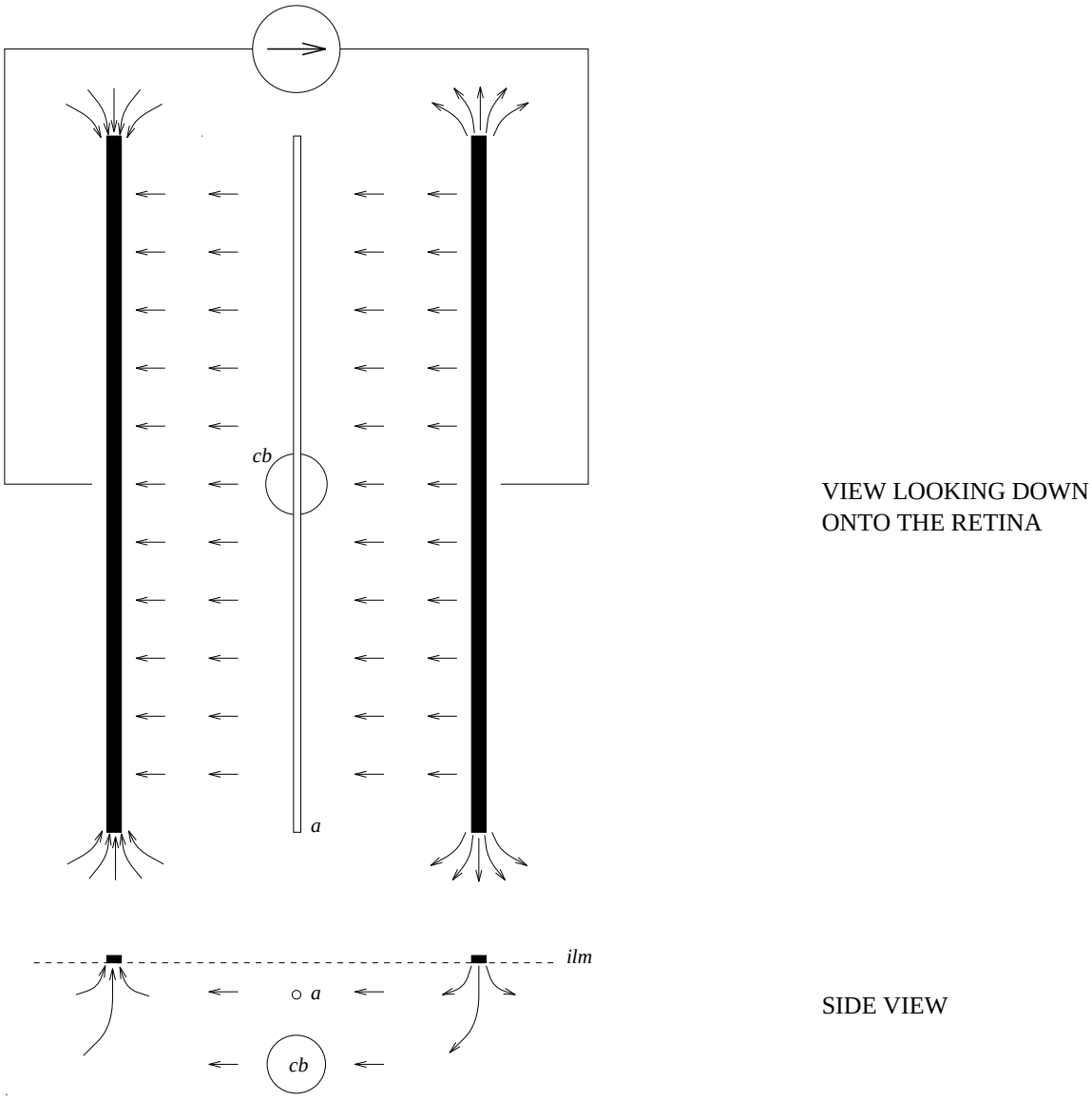

Figure 4-2: Schematic drawing of parallel wire electrode. Hypothesized electric field lines, including fringing, are drawn in. Abbreviations: *a* - axon; *cb* - cell body; *ilm* - inner limiting membrane.

this material were cut so that the conductor length was at least 2.5 times the conductors spacing (see Table 4.1 and Figure 4-4b for a complete specification of electrode dimensions). The width of the wires themselves was 5μm in all cases.

Early electrode designs used a copper-clad insulator to obtain the geometry of Figure 4-2. This material was abundantly available at Lincoln and could easily be cut into thin strips using a metal shear. However, copper may react with tissue and produce cell destruction when used in long-term experiments [12]. Even though our experiments were short-term (12 hours at most) in nature, we decided to use gold because it is considered "biologically inert" and therefore less likely to produce tissue damage.

A significant disadvantage of gold is that it is relatively soft. It was often found during electrode construction that the gold had been smeared or deformed in some way, either in the process of being cut by the wafer saw or during tip grinding. If the deformation was severe enough to obscure the basic parallel conductor geometry, the electrode was discarded.

In addition to gold, several other metals are considered biologically safe, including platinum, silver, stainless steel, and tantalum [12, 16]. Of these, only gold was readily available in the conductor-insulator-conductor form described above.

2. **Bond copper wires to the strip.** Insulated copper wires were stripped of their insulation at one end and soldered to either side of the strip obtained in step 1. Electrical contacts were tested by placing an ohm-meter between each wire (insulation removed at the other end as well) and the corresponding conductor, as depicted in Figure 4-3.2. If the resistance was small (10Ω or less) and the solder joint was mechanically robust, good electrical contact was assumed. Also, the resistance between the two wires was checked. If this resistance was large (off the scale of the ohm-meter), it was assumed that the two poles of the electrode weren't shorted together.

3. **Fill a glass tube with liquid epoxy.** A glass capillary tube (Drummond Scientific Co., Broomall, PA[1]) was then filled with Clear 2-Ton Epoxy (True Value Hardware, Cambridge, MA). The liquid (uncured) epoxy was drawn into the thin capillary tube by suction, as shown in Figure 4-3.3. A hypodermic needle of suitable diameter was attached to a syringe and inserted into the tube. Duct tape (not shown) was then wrapped around the base of the hypodermic and adjacent end of the glass tube to form an air-tight seal. Pulling back on the plunger of the syringe created a pressure vacuum inside of the capillary tube, drawing the epoxy up into it.

   Glass capillary tubing was used in the construction of the electrodes for a several reasons. First, encapsulating the conductor-insulator-conductor strip in the tube provided a straightforward way to electrically insulate its side faces from one another. Filling the space between the tube and the strip with epoxy (a good insulator) assured that there were no conductance paths between the side faces. This was done to prevent such conductance paths from shunting current away from the electrode tip. Alternatively, the strip could have been coated by dipping it in epoxy or some other insulator. This was tried with some success, but in general the insulated strip

[1]Three sizes, each specified by an inner diameter (*id*) and an outer diameter (*od*) listed in Table 4.1. The corresponding capillary tube volumes were 25, 50, and 100μL.

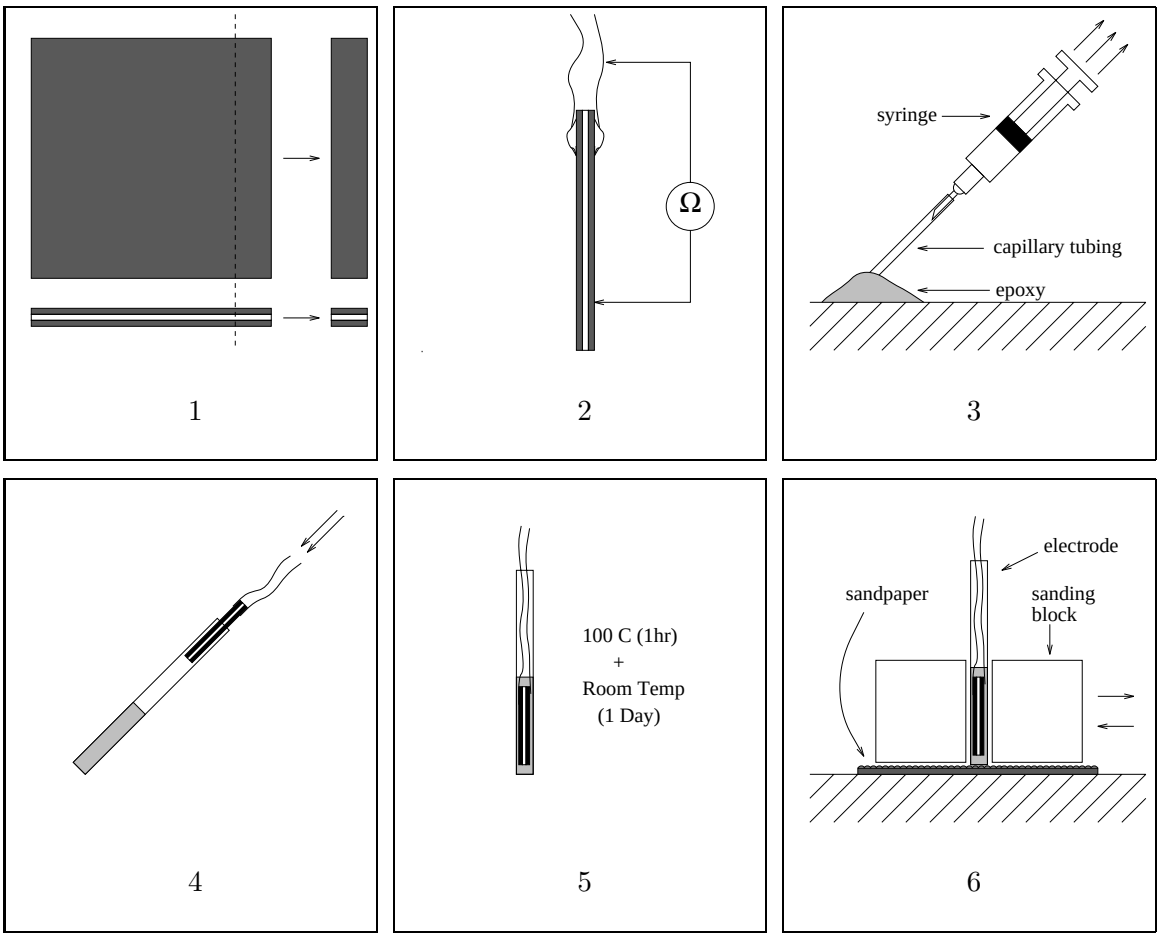

Figure 4-3: Electrode construction step by step. Not drawn to scale.

was difficult to work with due to its irregular shape. The second reason for using the glass tubing, then, was that its circular-cylindrical shape made it easy to work with. The sanding block in Figure 4-3.6, for example, was made by simply drilling a hole of suitable diameter in a block of teflon. Finally, the combined properties of small size, rigidity, and electrical insulation made the glass tubing advantageous. A small tube was needed for careful positioning of the electrode tip (see Chapter 5). In addition, a rigid tube was needed in order to have good control over the tip as it was lowered onto a preparation. Finally, an insulating tube was used to prevent stray coupling between electrode wires and their housing, which could have deformed the effective electrode geometry.

A disadvantage of using glass was that it was fragile and broke often. Metal tubes such as hypodermic needles are small, rigid, and more robust than glass. On the other hand, metal tubes conduct electricity, and were considered undesirable based on the reasoning above.

4. **Insert the strip.** The strip prepared previously was then inserted in the tube as shown in Figure 4-3.4. Though the strip was somewhat shorter than the tube, it

Design	d (μm)	l (μm)	id (μm)	od (μm)
1	127	572	660	991
2	254	635	736	1080
3	254	889	991	1370

Table 4.1: Electrode tip dimensions for three designs. d - conductor spacing; l - conductor length; id - inner diameter of the glass capillary tube; od - outer diameter of the capillary tube.

could be inserted far into the tube by pushing on the attached wires. A small epoxy-filled gap was left between the end of the strip and the end of the tube, as shown in Figure 4-3.5. This was done because bubbles often formed in the epoxy at the end of the tube as it cured. A small distance away from the end of the tube, the epoxy cured more uniformly, filling the space between the strip and the glass.

5. **Cure the epoxy.** The glass capillary tube, epoxy, and strip were then heated in an oven at 100°C for an hour. This helped to speed the curing time of the epoxy. After the tube was taken out of the oven, it was stored at room temperature for an additional 24 hours to insure that the epoxy had cured completely.

6. **Grind and polish the tip.** Once the epoxy was dry, it could be ground down with sandpaper. Using a sanding block as depicted in Figure 4-3.6, the end of the electrode was sanded at a right angle until the edge of the conductor-insulator-conductor sandwich could be clearly seen under a microscope. At this point, the tip of the electrode was polished by sanding with increasingly finer grades of sandpaper.

   A hard-curing epoxy was required for this step. The Clear 2-Ton epoxy was chosen because, of the epoxies tested, it cured the hardest. Even so, this epoxy may not have been hard enough. When electrode tips were viewed under the microscope (as in Figure 4-4a), it sometimes appeared as if the epoxy had smeared over the conductor surface. In addition, as one might observe directly from Figure 4-4, the bits of visible sandpaper grit (see step 6) embedded in the cured epoxy indicate that it was still substantially deformable. Furthermore, after several hours of immersion in saline solution, the epoxy appeared to have deformed somewhat. This was evidenced by visible peaks or valleys in the formerly flat surface of the electrode tip. Despite complications with the epoxy, the electrode's ability to pass current was uncompromised in all cases.

Pictures were taken of some of the electrode tips upon completion. A example is shown in Figure 4-4a. Below the picture in Figure 4-4b is a schematic drawing of the tip. Electrode tips of three different dimensions were made. These are listed in Table 4.1

Electrodes were tested prior to animal experiments using the apparatus of Figure 4-5. A voltage waveform V_i was established across the terminals of the circuit by the signal generator, and the resulting current flow through the electrode (if any) was measured as a voltage V_r across a known resistance. This provided a second check (in addition to that performed in step 2) that the poles of the electrode were not shorted together: if

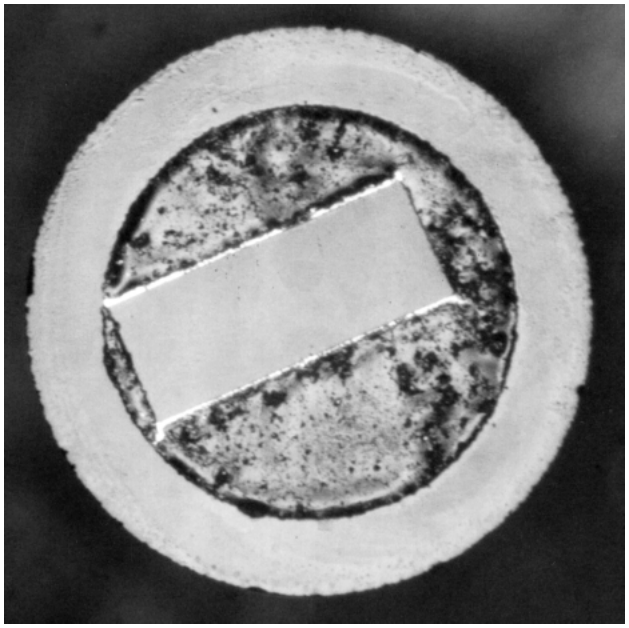

(a)

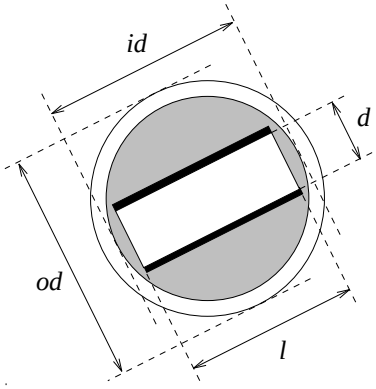

(b)

Figure 4-4: Electrode tip. (a) Photograph of a design 2 electrode; (b) Schematic of the tip with dimension variables labeled. The white annulus represents the edge of the capillary tube, which has inner diameter *id* and outer diameter *od*. The rectangle in the center represents a slice of conductor-insulator-conductor sandwich yielding wire length *l*. The white rectangle in the center is the fused silica, which had thickness *d*, and the thin black rectangles represent the gold wires, which in all cases were 5μm thick. The shaded region between the strip and the capillary tube represents the epoxy. Electrode tips of three different dimensions were made. These are listed in Table 4.1

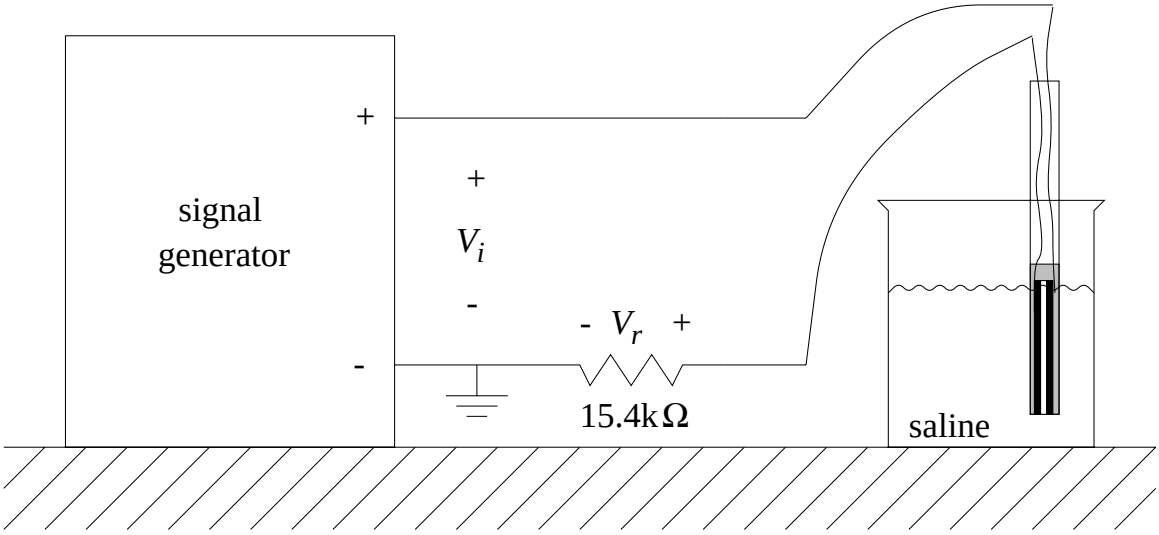

Figure 4-5: Apparatus for testing electrodes in saline.

the electrode was suspended in air, no direct current should flow between the poles of the electrode when it is connected to the signal generator. The apparatus of Figure 4-5 might also be used to determine the electrical characteristics of the electrode in physiological saline solution.

4.3 Predicting the electric field

Preliminary attempts have been made to model the electric fields produced in the retina by the electrodes constructed for this thesis. Such fields are produced by the flow of ions in the biological fluid. The ionic flow is made possible by electrochemical reactions at the electrode:solution interfaces. Our approach has neglected these interactions in the interest of simplicity. More detailed descriptions of electrode-surface reactions and related phenomena are found in [16, 17, 50, 56, 58].

To find the electric field produced by the electrode, Laplace's equation must be solved within some volume which contains the tip[2]. For the moment, let this volume be arbitrary, and consider a surface which bounds it. If either the potential on the surface (Dirichlet boundary condition) or the derivative of the potential normal to the surface (Neumann boundary condition) is specified for every point on the surface, then a unique solution for Laplace's equation exists within the volume.

Now assume that the electrode tip forms one side of the bounding surface. Because they are equipotentials, the conducting regions of the electrode tip are conveniently modeled using Dirichlet boundary conditions. Note that the electrode is symmetrical about a line parallel to and lying between the two wires. Due to this symmetry, the wires will be at

[2]As in Chapter 3, we assume that there are no fixed charges near the electrode, and that Laplace's equation will be solved within a material that is linear, isotropic, and homogeneous.

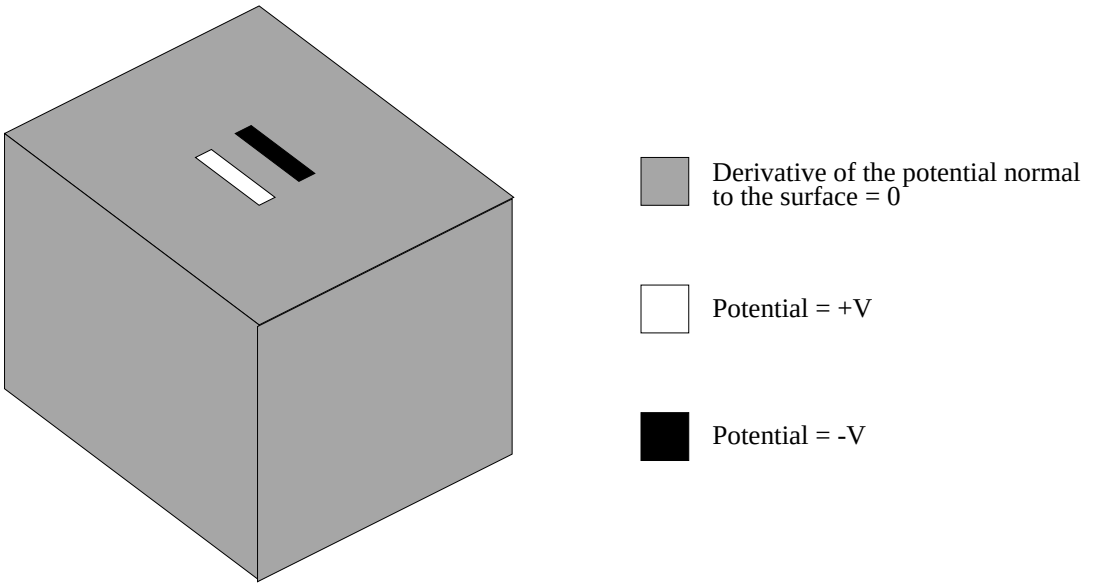

Figure 4-6: Model for predicting the electric fields generated using the stimulating electrode described in this chapter.

equal and opposite voltages when stimuli are applied. The epoxy and glass are modeled as perfect insulators through which no current will flow. This requires that the current density normal to the surface in such regions is zero. Since the normal current density is proportional to the normal derivative of the potential, Neumann boundary conditions are used to represent the non-conducting portions of the electrode tip. Assume further that the remaining portions of the bounding surface are far away from the bipolar electrode. Like the regions of the bounding surface representing insulators, no current will flow through these regions. Neumann boundary conditions are therefore established at these regions as well.

Laplace's equation subject to the boundary conditions described above does not lend itself readily to analytical techniques. However, we may be able to solve this problem efficiently using a numerical algorithm. To facilitate this process, the bounding surface is chosen to be a box. Our model for predicting the electric field produced by the electrode is shown in Figure 4-6. An algorithm for solving this problem has not yet been implemented.

Chapter 5

On experimental verification

Preliminary attempts were made to experimentally test the electrodes of chapter 4. A total of seven experiments were conducted. Two of these were performed by Dr. Ralph Jensen (Southern College of Optometry, Memphis, TN) using a small slice of the rabbit retina. This preparation has been used extensively for other retinal implant project experiments [64], and is described in detail elsewhere [27]. The remaining five experiments were performed by Dr. Lyle Borg-Graham (visiting scientist at MIT during the month of February, 1994; currently at the Institut Alfred Fessard, CNRS, Gif-sur-Yvette, France) and the author using an isolated turtle retina preparation, also described elsewhere [4].

This chapter is divided into three sections. In the first section, three hypotheses which might be tested in an experiment are presented. These will help to motivate the experimental procedures outlined in the second section. Results obtained using the methods described were on the whole inconclusive. This was due in part to the relatively small number of experiments conducted. More importantly, though, results were inconclusive due to several unresolved experimental issues. These will be described in the third section of the chapter. Such issues must be addressed in future experiments if the hypotheses are to be tested in a conclusive manner. For the most part, results from the experiments will not be presented.

5.1 Three hypotheses

It was argued in chapter 4 that the parallel wire electrode could be used to selectively stimulate cell bodies. This argument was based on a comparison made in section 3.4 for the parallel plate electrode. Two additional comparisons for the parallel plates were made in that section. These might also be applicable to the parallel wire electrode.

The comparisons assume that the spacing of the plates is much larger than the space constant of the axon. To a first approximation, this assumption might be modified for the electrodes of chapter 4 by requiring that the spacing of the *wires* is much larger than the space constant. Does this modified assumption hold? Using "typical" values for the electrical properties of nerve membranes, we calculated in chapter 3 that the length constant was about 112μm. From Table 4.1, we see that the wire spacing is just over one length constant for the design 1 electrode and about two length constants for designs 2 and 3. Thus, the assumption does not hold strictly for the electrodes designed in chapter 4.

To bring the electrodes in line with the assumptions of chapter 3, larger wire spacings could have been incorporated into the design. This would have required that the wire length also be larger (see section 4.1), and the resulting electrode tip would have increased